Majorana bound states in chains of interacting quantum dots

by William Samuelson

LUND
UNIVERSITY

Division of Solid State Physics and NanoLund

Thesis for the degree of
Master of Science in Engineering Physics

Supervisor: Martin Leijnse
Co-supervisor: Viktor Svensson

Examiner: Carina Fasth

June 5, 2023

Abstract

This thesis concerns the creation of Majorana bound states (MBSs) – a type of condensed matter excitations theorized to have exotic and technologically valuable properties. In particular, they could be used to store and manipulate quantum information in a protected way, forming the building blocks of a topological quantum computer. The search for MBSs has been intense since it was realized that they could be created in superconductor-semiconductor hybrid structures, such as long chains of quantum dots separated by superconductors. Majorana bound states can even appear in two-site chains, although called "poor man's" MBSs since they only appear at fine-tuned sweet spots and hence lack the protection standard MBSs offer. However, they share all other properties of MBSs, making the short quantum dot chains appealing for studying their exotic physics. In this thesis, we study the platform proposed in Ref. [1], consisting of a short chain of quantum dots where each dot is coupled to a separate superconductor. However, we consider Coulomb interactions in the system, which were neglected in the original work. We develop MBS quality measures to determine that Coulomb interactions do not destroy the possibility of creating MBSs. Furthermore, we use the quality measures to conclude that adding more sites to the chain does not necessarily improve the MBS quality. Finally, we suggest that control of the superconducting phases can be used to fine-tune the system to the sweet spot. In conclusion, this thesis finds that the quantum dot chain is a relevant platform for creating poor man's MBSs.

Populärvetenskaplig sammanfattning

Majorana-tillstånd i kedjor av kvantprickar

Majorana-tillstånd är exotiska kvanttillstånd som tros kunna användas för att lagra och manipulera kvantinformation på ett helt nytt och robust sätt. Skapandet av Majorana-tillstånd skulle inte bara skriva fysikhistoria utan också revolutionera utvecklingen av kvantdatorer.

Vid mycket låga temperaturer kan vissa metaller gå igenom en fasövergång och bli supraledande. I ett sådant tillstånd parar alla elektroner ihop sig i så kallade Cooper-par. Tillsammans bildar den enorma mängden par (i storleksordningen Avogadros tal) en koherent vågfunktion, vilket gör att elektronerna kan flöda helt utan motstånd. Supraledning är på så sätt ett tillstånd där kvantmekaniken gör sig till synes även i vår makroskopiska värld. Detta beteende hos elektroner i supraledare skiljer sig helt från ”vanliga” material, som metaller och halvledare, där elektroner beter sig mer individuellt. I halvledare är istället elektronerna bundna till atomkärnor, förutom ett fåtal elektroner som fått tillräckligt med termisk energi för att kunna färdas genom halvledaren. Anledningen till halvledarnas tekniska användbarhet och den gigantiska halvledarindustrin är att deras elektroniska egenskaper kan förändras genom att införa föroreningar i halvledaren. Det går till och med att skapa konstgjorda atomer av halvledare, så kallade kvantprickar. I kvantprickar går det att precist avgöra och justera antalet elektroner. Därför är de mycket användbara för att undersöka kvantmekaniska koncept och utveckla ny typ av kvantteknologi som utnyttjar kvantmekanik för att utföra uppgifter effektivt eller med hög precision.

I början av 2010-talet insåg man att kombinationen av halvledare och supraledare kunde möjliggöra formationen av så kallade Majorana-tillstånd. Stora satsningar har gjorts för att skapa dessa exotiska tillstånd och experimentella tecken av dem har uppmätts, men än så länge saknas det övertygande bevis. Det finns två anledningar till att det satsas så mycket på forskningen kring Majorana-tillstånd. För det första förväntas de kunna lagra kvantinformation som inte blir förvrängd av störningar

på systemet. För det andra beter sig Majorana-tillstånd speciellt när man byter plats på dem. Vanliga partiklar, som elektroner, återgår till sitt ursprungstillstånd efter att de har bytt plats med en annan elektron två gånger. Ett system med Majorana-tillstånd däremot, tros hamna i ett helt annat tillstånd efter platsbyten. Genom att kontrollerat byta plats på Majorana-tillstånd kan man därför manipulera kvantinformationen som är lagrad i dem, och på så sätt implementera en kvantdator.

I denna avhandling studerar jag ett system där Majorana-tillstånd förväntas finnas enligt tidigare forskning. Systemet består av en kedja av kvantprickar där varje prick är kopplad till en supraledare. Vid stora magnetiska fält och efter finjustering av systemets parametrar, uppstår två Majorana-tillstånd, en på vardera änden av kedjan. Till skillnad från tidigare forskning av systemet har jag inkluderat växelverkan mellan elektroner i modellen. Under arbetets gång har jag, analytiskt och med hjälp av en dator, undersökt hur denna växelverkan mellan elektroner i kvantprickarna och längden på kedjan påverkar Majorana-tillstånden. Resultaten visar att Majorana-tillstånden kan bli av både sämre och bättre kvalitet av växelverkan, men att de ändå alltid går att hitta. Att öka längden på kedjan verkar inte nödvändigtvis öka kvaliteten på Majorana-tillstånden. Ett annat viktigt resultat från arbetet är att man kan använda supraledarnas faser för att finjustera systemet så att Majorana-tillstånd uppstår. Sammanfattningsvis är kedjan av kvantprickar ett relevant alternativ för att skapa och detektera Majorana-tillstånd.

Contents

I

Introduction

Superconductivity is a phase of matter that arises in certain metallic elements at low temperatures. In the superconducting state, all electrons pair up in so-called Cooper pairs, forming a macroscopic and coherent quantum wavefunction [2]. This allows them to move with perfect conductance through the superconductor. On the other hand, semiconductors have a conductance intermediate to metals and insulators. Most electrons in a semiconductor are tightly bound to the nuclei, and only a few electrons have enough thermal energy to move through the material, although with a finite resistance [3]. However, the advances in fabrication and processing within semiconductor technology have allowed for precise control of the properties of nanoscale structures; even forming tiny artificial atoms, called quantum dots, is now standard practice [4]. In the marriage between superconductors and semiconductors lies rich and exotic physics waiting to be discovered. In the early 2010s, it was realized that the combination of superconductors and semiconductors could be used to engineer topological superconductors hosting so-called Majorana bound states (MBSs) [5]. The successful detection and control of MBSs would allow for the exploration of novel phenomena in fundamental physics, most notably non-Abelian exchange statistics, and the possibility to implement a robust, topological quantum computer [6, 7]. Therefore, the search for MBSs has been intense, both from leading research groups and from industry [8].

One of the platforms most studied for creating MBSs is semiconducting nanowires strongly coupled to superconductors [5]. Two MBSs are expected to form in such systems, one at each end of the wire. In 2012, the first signs of MBSs in nanowires were detected [9], see also Refs. [10–12] for further examples. However, it has become increasingly clear that similar signals could be generated by other effects not originating from the formation of MBSs [13–15]. Therefore, it is still controversial whether they have been detected. To find more conclusive evidence, there has lately been a push to study simpler systems where MBSs are expected to form. The

minimal system required to have MBSs is a two-site version of a toy-model Kitaev proposed in 2001 – the Kitaev chain [16]. A two-site Kitaev chain can be realized using two quantum dots separated by a superconductor [17, 18], and experimental signs of MBSs in such a system were found in 2023 [19]. The MBSs appearing in short Kitaev chains are called poor man's MBSs since they lack the extent of protection regular MBSs have against perturbations. Instead, the poor man's MBSs appear when the system is fine-tuned to a "sweet spot" in parameter space. Except for the lesser amount of protection, poor man's MBSs share all other properties of regular MBSs, such as their non-Abelian exchange statistics. The relatively simple setup required to create poor man's MBSs is, therefore, an attractive way to study their exotic physics.

In this thesis, we analyze a chain of quantum dots with the potential to create poor man's MBSs. Instead of having a superconductor between the quantum dots like the original proposal and the recent experiments, we have studied a system where each dot is coupled to its own superconductor. This system was proposed in Ref. [1], where it was shown that an effective Kitaev chain description emerges for large magnetic fields. However, electron-electron interactions were not considered, which are expected to be important in the system. In this work, we include interactions between electrons on the same site and neighboring sites. To compare the situation with and without interactions, we develop an MBS quality measure. Using the measure, we investigate how interactions and chain length impact the quality of MBSs. Finally, we discuss how the system could be tuned to the sweet spot using the phases of the superconductors.

The aim of the thesis is to investigate an alternative platform for studying poor man's MBSs. The system we consider is simpler to implement than the original poor man's proposition since the quantum dots are directly next to each other. However, it is more sensitive to interactions between electrons on neighboring sites, which are shielded by the superconductors in the original platform. Therefore, investigating the interdot Coulomb interactions' impact on the MBSs is essential to conclude our model's relevance as an alternative to the original poor man's system. Furthermore, determining if longer chains increase the MBS quality will help experimentalists to know if adding more dots to their setups is worth the extra effort.

The structure of the thesis is as follows. First, in Chapter II, we provide a background of the main subjects of the thesis – quantum dots, conventional superconductivity, the superconducting proximity effect, and topological superconductivity. Next, we introduce the model of the quantum dot chain and derive the effective Kitaev chain parameters in Chapter III. Then, in Chapter IV, we discuss the methodology of the thesis work. The results of the thesis is presented in Chapter V. Finally, we conclude in Chapter VI by discussing the results and giving an outlook on future work.

II

Background

This chapter is devoted to establishing a proper background for the rest of the thesis. To begin with, we introduce quantum dots and discuss how to model them. Next, we cover superconductivity and standard theoretical tools for analyzing superconductors, such as the Bardeen-Cooper-Schrieffer theory. In Section II.3, we combine the previous two sections by placing a superconductor near a quantum dot. To understand the exciting physics arising in such systems, we first review the superconducting proximity effect, which explains how superconductivity tends to leak into nearby normal-state materials. Then, we look at the specific case when the proximitized material is a quantum dot. Theoretically, chains of quantum dots proximitized by superconductors can host MBSs. In Section II.4, we introduce Majorana physics and topological superconductivity with a famous toy model, the Kitaev chain. Finally, we discuss the notion of poor man's Majorana bound states and possible quality measures for such states. Throughout the thesis, we have set the reduced Planck's constant to unity ($\hbar = 1$).

II.1 Quantum dots

In low-dimensional materials, electrons are confined in one or more dimensions, leading to quantum effects that strongly influence the electrons' behavior. In quantum dots, the electrons are tightly confined in all three spatial dimensions. This leads to electronic properties similar to those of atoms, most notably, a quantized energy spectrum and the so-called charging energy – the additional energy required to add an electron to the dot due to Coulomb repulsion [4, 20]. To access quantum phenomena in quantum dots, the confinement length needs to be small in comparison to the thermal wavelength of the electrons. Therefore, the size of a quantum dot is typically tens of nanometres, and experiments are usually performed at cryogenic temperatures [4]. Nowadays, there are many different ways to construct such tiny

islands of electrons. One technique is to first restrict the electrons to one or two dimensions in semiconducting nanowires or two-dimensional electron gases and then electrostatically confine them in the remaining directions with nanoscale electrodes called gates. Chains of two quantum dots, forming artificial molecules, can be manufactured with the same techniques [4, 21].

Typically, quantum dot setups have additional gates that can be used to fine-tune the energy levels and precisely control the number of electrons on the dot. Quantum dots are hence an excellent testing ground for fundamental quantum physics. In the following section, we introduce how to model chains of quantum dots, which will be used throughout the thesis.

II.1.1 Modeling quantum dot chains

As discussed above, the energy levels of a quantum dot are quantized and can be well separated. One common assumption when modeling a quantum dot system is that the spacing between energy levels is large in comparison with the other energy scales of the system. Then, one needs only to include one energy level per quantum dot. This approximation will be used throughout this thesis. A Hamiltonian describing a chain of N quantum dots can, in the language of second quantization, be written as

$$H_{\text{chain}} = \sum_{j=1,s}^{N} \mu_{j,s} n_{j,s} + \sum_{j=1,s}^{N-1} [w_j d^\dagger_{j+1,s} d_{j,s} + \text{H.c.}] + \sum_{j=1}^{N} U_{\text{intra}} n_{j\uparrow} n_{j\downarrow} + \sum_{j=1}^{N-1} U_{\text{inter}} N_j N_{j+1}. \tag{II.1}$$

Here, $d^\dagger_{j,s}$ creates an electron on quantum dot j with spin $s \in \{\uparrow, \downarrow\}$ and $d_{j,s}$ is the corresponding annihilation operator. Furthermore, $n_{j,s} = d^\dagger_{j,s} d_{j,s}$ counts the number of electrons at site j with spin s, and $N_j = n_{j\uparrow} + n_{j\downarrow}$ counts the total number of electrons at site j. The first term hence adds together the single-particle energies $\mu_{j,s}$ for each occupied state. Note that the energy is, in general, spin-dependent, taking into account e.g., magnetic fields. The second term represents tunneling between sites j and $j+1$, with a tunneling amplitude w_j. Finally, Coulomb interactions between electrons on the same dot (intradot) and on neighboring dots (interdot) are taken into account by the last two terms. The Hamiltonian in Eq. (II.1) is the starting point when we model the system in Chapter III.

II.2 Superconductivity

In 1911, the Dutch physicist Heike Kamerlingh Onnes recorded the first proof of superconductivity while measuring the resistivity of mercury at cryogenic temperatures [2]. When the mercury reached a temperature of 4.2 K, Onnes noticed that the resistivity suddenly dropped to zero. While not knowing it at the time, Onnes had

witnessed a phase transition to a superconducting state with perfect conductance. However, it took 46 years from Onnes's famous experiments until Bardeen, Cooper, and Schrieffer (BCS) proposed the complete microscopic theory of superconductivity in 1957 [22]. A year later, Bogoliubov and Valatin independently set the idea on firmer grounds by introducing the Bogoliubov (-Valatin) transformation [23, 24], which later developed into the Bogoliubov-de Gennes (BdG) formalism [25]. In this section, these essential theoretical tools for describing superconductivity are reviewed.

II.2.1 Bardeen-Cooper-Schrieffer theory

A year before the BCS paper, Cooper showed that electrons can form so-called Cooper pairs that lower the energy of the normal state Fermi sea in the presence of a net attractive interaction between the paired electrons [26]. But how could such an attractive interaction occur? Electrons are charged particles, and due to the Coulomb interaction, they repel each other. A few years before the BCS paper, experiments by Maxwell and Reynolds et al. [27, 28] showed that the superconducting transition temperature of mercury varies between isotopes. The conclusion was that superconductivity arises from interactions between electrons and lattice vibrations. It can be shown that such interactions can result in an attractive net attraction between a pair of electrons, the intuitive idea being that the first electron attracts the positive ions close to it, which then attract the second electron [2]. Cooper's proposition of paired electrons hence stood on firm experimental ground.

BCS took the Cooper pairing idea further by forming an ansatz for the ground state of a superconductor:

$$|\psi_G\rangle = \prod_{\boldsymbol{k}} (|u_{\boldsymbol{k}}| + |v_{\boldsymbol{k}}| e^{i\Phi} c^\dagger_{\boldsymbol{k}\uparrow} c^\dagger_{-\boldsymbol{k}\downarrow}) \, |0\rangle \, , \tag{II.2}$$

where $|0\rangle$ is the vacuum state, $u_{\boldsymbol{k}}$ and $v_{\boldsymbol{k}}$ are variational coefficients to be determined, and $c^\dagger_{\boldsymbol{k}s}$ is the creation operator for an electron with momentum $\boldsymbol{k}$ and spin s. Furthermore, Φ will turn out to describe the *phase* of the superconductor, which becomes important to consider in systems with several superconductors. The BCS ansatz can be understood as follows: For each momentum $\boldsymbol{k}$, a Cooper pair of electrons $(\boldsymbol{k}\uparrow, -\boldsymbol{k}\downarrow)$ is occupied with probability $|v_{\boldsymbol{k}}|^2$ and unoccupied with probability $|u_{\boldsymbol{k}}|^2$. Assuming that the interactions that are important for superconductivity are between the Cooper paired electrons, the Hamiltonian of the superconductor is given by

$$H_{\mathrm{SC}} = \sum_{\boldsymbol{k}s} \epsilon_{\boldsymbol{k}} c^\dagger_{\boldsymbol{k}s} c_{\boldsymbol{k}s} + \sum_{\boldsymbol{k}\boldsymbol{l}} V_{\boldsymbol{k}\boldsymbol{l}} c^\dagger_{\boldsymbol{k}\uparrow} c^\dagger_{-\boldsymbol{k}\downarrow} c_{-\boldsymbol{l}\downarrow} c_{\boldsymbol{l}\uparrow}, \tag{II.3}$$

where $\epsilon_{\boldsymbol{k}}$ is the single particle energy of an electron with momentum $\boldsymbol{k}$. The interaction term in Eq. (II.3) can be seen as the scattering of a Cooper pair from momenta

$(\boldsymbol{l}, -\boldsymbol{l})$ to $(\boldsymbol{k}, -\boldsymbol{k})$, with $V_{\boldsymbol{kl}}$ describing the attractive interaction between the Cooper paired electrons discussed above.

Minimizing the energy of the state in Eq. (II.2) with respect to H_{SC}, the variational coefficients $u_{\boldsymbol{k}}$ and $v_{\boldsymbol{k}}$ are obtained. By inserting the coefficients into Eq. (II.2), the energy of the BCS ansatz can be calculated, which shows that it indeed has lower energy than the Fermi-sea [2]. The ground state of a superconductor hence consists of a macroscopic wavefunction of Cooper pairs. The BCS paper finally made it possible to calculate the properties of superconductors from a microscopic theory and is one of the 20th century's major breakthroughs in physics. However, to deal with excited states of the superconductor, another approach is better suited than the variational approach BCS used – the Bogoliubov transformation.

II.2.2 The Bogoliubov transformation

The interaction term in the Hamiltonian in Eq. (II.3) is difficult to deal with since it contains products of four operators. With mean-field arguments, however, it is possible to reduce the product of four operators into terms of two operators. Since the BCS ground state in Eq. (II.2) is a superposition of states with different particle numbers, operators like $c_{-\boldsymbol{k}\downarrow}c_{\boldsymbol{k}\uparrow}$ can have non-zero expectation values. Furthermore, since the number of particles involved in the state is macroscopic, we can expect that the fluctuations around these expectation values are small [2]. We can then form

$$\begin{aligned} c_{-\boldsymbol{k}\downarrow}c_{\boldsymbol{k}\uparrow} &= \langle c_{-\boldsymbol{k}\downarrow}c_{\boldsymbol{k}\uparrow}\rangle + (c_{-\boldsymbol{k}\downarrow}c_{\boldsymbol{k}\uparrow} - \langle c_{-\boldsymbol{k}\downarrow}c_{\boldsymbol{k}\uparrow}\rangle) \quad \text{and} \\ c^\dagger_{\boldsymbol{k}\uparrow}c^\dagger_{-\boldsymbol{k}\downarrow} &= \langle c^\dagger_{\boldsymbol{k}\uparrow}c^\dagger_{-\boldsymbol{k}\downarrow}\rangle + (c^\dagger_{\boldsymbol{k}\uparrow}c^\dagger_{-\boldsymbol{k}\downarrow} - \langle c^\dagger_{\boldsymbol{k}\uparrow}c^\dagger_{-\boldsymbol{k}\downarrow}\rangle), \end{aligned} \tag{II.4}$$

and neglect terms bilinear in the fluctuation terms in the parentheses. The Hamiltonian in Eq. (II.3) then turns into the mean-field Hamiltonian

$$H_{\mathrm{MF}} = \sum_{\boldsymbol{k}s} \xi_{\boldsymbol{k}} c^\dagger_{\boldsymbol{k}s}c_{\boldsymbol{k}s} - \sum_{\boldsymbol{k}} (\Delta_{\boldsymbol{k}} c^\dagger_{\boldsymbol{k}\uparrow}c^\dagger_{-\boldsymbol{k}\downarrow} + \Delta^*_{\boldsymbol{k}} c_{-\boldsymbol{k}\downarrow}c_{\boldsymbol{k}\uparrow}) \tag{II.5}$$

where $\xi_{\boldsymbol{k}} = \epsilon_{\boldsymbol{k}} - \mu$ is the single particle energy with respect to the Fermi level μ and

$$\Delta_{\boldsymbol{k}} = -\sum_{\boldsymbol{l}} V_{\boldsymbol{kl}} \langle c_{-\boldsymbol{k}\downarrow}c_{\boldsymbol{k}\uparrow}\rangle , \tag{II.6}$$

is the superconducting pairing amplitude, which has to be calculated self-consistently. Note that in Eq. (II.5), we have neglected constant terms since they just shift all energies. This will be done throughout this thesis.

As desired, the new Hamiltonian in Eq. (II.5) is now bilinear in the electron operators. Bogoliubov and Valatin realized that such a Hamiltonian could be diagonalized by transforming the operators $c_{\boldsymbol{k}s}$ into new fermionic operators, $\gamma_{\boldsymbol{k}0}$ and $\gamma_{\boldsymbol{k}1}$ [23, 24]. The appropriate transformation is given by

$$c_{\boldsymbol{k}\uparrow} = u^*_{\boldsymbol{k}}\gamma_{\boldsymbol{k}0} + v_{\boldsymbol{k}}\gamma^\dagger_{\boldsymbol{k}1} \tag{II.7a}$$

$$c^\dagger_{-\boldsymbol{k}\downarrow} = -v^*_{\boldsymbol{k}}\gamma_{\boldsymbol{k}0} + u_{\boldsymbol{k}}\gamma^\dagger_{\boldsymbol{k}1} \tag{II.7b}$$

where $u_{\boldsymbol{k}}$ and $v_{\boldsymbol{k}}$ will turn out to be the same as $u_{\boldsymbol{k}}$ and $v_{\boldsymbol{k}}$ in the variational approach. Inserting Eq. (II.7) in Eq. (II.5) and imposing the requirement that the Hamiltonian is diagonal, i.e., only contain terms of the form $\gamma^\dagger_{\boldsymbol{k}}\gamma_{\boldsymbol{k}}$, the mean-field Hamiltonian then reduces to

$$H_{\mathrm{MF}} = \sum_{\boldsymbol{k}} E_{\boldsymbol{k}}(\gamma^\dagger_{\boldsymbol{k}0}\gamma_{\boldsymbol{k}0} + \gamma^\dagger_{\boldsymbol{k}1}\gamma_{\boldsymbol{k}1}), \tag{II.8}$$

where $E_{\boldsymbol{k}} = \sqrt{\xi^2_{\boldsymbol{k}} + |\Delta_{\boldsymbol{k}}|^2}$ [2].

By performing a Bogoliubov transformation to a basis of the so-called quasiparticle operators $\gamma_{\boldsymbol{k}0}$ and $\gamma_{\boldsymbol{k}1}$, the mean-field Hamiltonian in Eq. (II.8) becomes simple. The absence of quasiparticles corresponds to the BCS ground state in Eq. (II.2), and excited states contain one or more quasiparticles. Since the energy of a quasiparticle is $E_{\boldsymbol{k}} = \sqrt{\xi^2_{\boldsymbol{k}} + |\Delta_{\boldsymbol{k}}|^2}$, the minimum energy required to excite the system is $|\Delta_{\boldsymbol{k}}| > 0$. The parameter $\Delta_{\boldsymbol{k}}$ hence plays the role of an energy gap in the density of states in the superconductor, see Fig. II.1. The Cooper pairs of the superconductor live at zero energy.

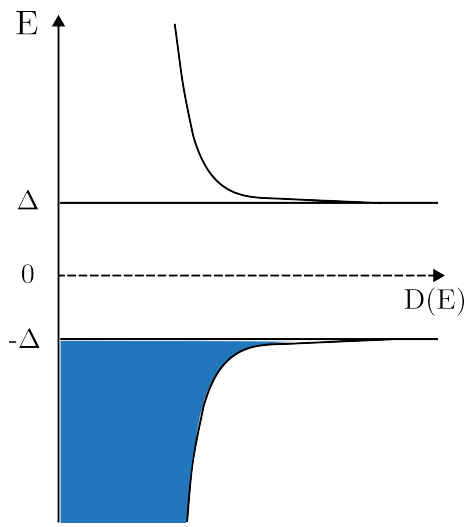

Figure II.1: The density of states D of quasiparticles in a superconductor on the horizontal axis with energy E on the vertical axis. At zero temperature, the quasiparticle states are filled up to $E = -\Delta$ and unoccupied above the gap, with no available states in between.

As we have seen in the derivation above, the idea behind the Boguliubov transformation is to transform the original operators such that excitations can be described as the occupation of quasiparticle states. The Bogoliubov transformation is not only used within bulk superconductivity but is a useful tool in general when the Hamiltonian is quadratic in its creation and annihilation operators. In the next section, a method of finding the appropriate transformation is reviewed, the BdG formalism.

II.2.3 Bogoliubov-de Gennes formalism

Inverting Eq. (II.7), we can express the quasiparticle operators in terms of the original operators and see that they consist of superpositions of particles and holes:

$$\gamma_{\boldsymbol{k}0} = u_{\boldsymbol{k}} c_{\boldsymbol{k}\uparrow} - v_{\boldsymbol{k}} c^\dagger_{-\boldsymbol{k}\downarrow} \tag{II.9a}$$

$$\gamma_{\boldsymbol{k}1} = u_{\boldsymbol{k}} c_{-\boldsymbol{k}\downarrow} + v_{\boldsymbol{k}} c^\dagger_{\boldsymbol{k}\uparrow}. \tag{II.9b}$$

For an arbitrary quadratic Hamiltonian, we would like to find the corresponding transformation. This can be done in a systematic way in the BdG formalism, which will be described in what follows and is based on Ref. [25]. We consider a Hamiltonian H, quadratic in the operators $c_1, c_2, \dots c_N$ and their corresponding creation operators. A general transformation of the type in Eq. (II.9) to quasiparticle operators $\{a_j, a_j^\dagger\}_j$ is given by

$$a_n = \sum_j u^*_{nj} c_j + v^*_{nj} c^\dagger_j, \quad a^\dagger_n = \sum_j u_{nj} c^\dagger_j + v_{nj} c_j. \tag{II.10}$$

This can be written in matrix notation as $\Phi = M\Psi$, with

$$\begin{gathered} \Phi = (a_1, \dots, a_N, a_1^\dagger, \dots, a_N^\dagger)^T, \quad \Psi = (c_1, \dots, c_N, c_1^\dagger, \dots, c_N^\dagger)^T, \\ M = \begin{pmatrix} U^* & V^* \\ V & U \end{pmatrix}, \end{gathered} \tag{II.11}$$

and where U and V contains the coefficients u_{nj} and v_{nj} from Eq. (II.10). Furthermore, we want the new quasiparticles in Eq. (II.10) to obey the fermionic anti-commutation relations. This requires M to be unitary.

To find the transformation matrix M, we first use Ψ to rewrite the Hamiltonian as

$$H = \frac{1}{2} \Psi^\dagger h_{\mathrm{BdG}} \Psi, \tag{II.12}$$

where h_{BdG} is the Bogoliubov-de Gennes Hamiltonian. Diagonalizing h_{BdG} leads to the so-called BdG equations

$$h_{\mathrm{BdG}} \begin{pmatrix} \tilde{u}_n \\ \tilde{v}_n \end{pmatrix} = E_n \begin{pmatrix} \tilde{u}_n \\ \tilde{v}_n \end{pmatrix}, \tag{II.13}$$

where $\tilde{u}_n$ and $\tilde{v}_n$ are N-component column vectors, together forming the nth eigenvector to h_{BdG} with energy E_n.

The BdG Hamiltonian has a certain property called particle-hole symmetry. For superconductors, the particle-hole symmetry operator is given by an anti-unitary operator $\mathcal{P} = \tau_x \mathcal{K}$, where τ_x is the first Pauli matrix acting on the blocks of annihilation and creation operators, and $\mathcal{K}$ is the operator for complex conjugation [29]. The particle-hole symmetry of h_{BdG} is written as

$$\mathcal{P} h_{\mathrm{BdG}} \mathcal{P}^{-1} = -h_{\mathrm{BdG}}, \tag{II.14}$$

which implies that an eigenstate $(u_n, v_n)^T$ with energy E_n will have a partner $(v_n^*, u_n^*)^T$ with energy $-E_n$. It is hence enough to consider the positive energy eigenvectors. Since h_{BdG} is Hermitian, we can use the eigenvectors to form a unitary transformation matrix Γ which diagonalizes h_{BdG}:

$$\Gamma = \begin{pmatrix} \tilde{u}_1 & \dots & \tilde{u}_N & \tilde{v}_1^* & \dots & \tilde{v}_N^* \\ \tilde{v}_1 & \dots & \tilde{v}_N & \tilde{u}_1^* & \dots & \tilde{u}_N^* \end{pmatrix} \implies h_{\text{BdG}} = \Gamma D \Gamma^\dagger, \tag{II.15}$$

where $D = \text{diag}(E_1, \dots, E_N, -E_1, \dots, -E_N)$. Inserting the transformation into Eq. (II.12) results in

$$H = \frac{1}{2}\Psi^\dagger(\Gamma D \Gamma^\dagger)\Psi = \frac{1}{2}(\Gamma^\dagger\Psi)^\dagger D(\Gamma^\dagger\Psi). \tag{II.16}$$

Now we claim that the appropriate transformation matrix is given by $M = \Gamma^\dagger$ and that the quasiparticles hence are given by $\Phi = \Gamma^\dagger\Psi$. Note that $\Gamma^\dagger$ is unitary and has the appropriate structure described in Eq. (II.11). Assuming that this is the correct transformation, we get

$$H = \frac{1}{2}\Phi^\dagger D \Phi = \frac{1}{2}\sum_j E_j a_j^\dagger a_j - E_j a_j a_j^\dagger = \sum_j E_j a_j^\dagger a_j + \text{const.}, \tag{II.17}$$

and hence, the assumption works, and we have found the new operators $\{a_j, a_j^\dagger\}_j$ given by $\Phi = \Gamma^\dagger\Psi$ which diagonalize the Hamiltonian.

Since Ψ has $2N$ elements, h_{BdG} is a $2N \times 2N$ matrix and scales linearly with the number of particles. When dealing with multiple particles, this improves computation time drastically compared to using a many-body basis, which scales exponentially with the number of particles. However, when there are explicit interactions in the system, one must revert to the many-body basis. One particular application of the Boguliobov transformation and BdG formalism can be seen in Chapter III.

II.3 The superconducting proximity effect

The superconducting proximity effect describes phenomena when a "normal" non-superconductive material (N) is coupled to a superconductor (S) such that electrons can be transferred between the two materials. As we have seen in Section II.2, the electrons in a superconductor form Cooper pairs and are hence ordered in a completely different way than in a normal material. Because of the plane-wave behavior of electrons in bulk materials, the properties of the electrons cannot change infinitely quickly. Intuitively, it is hence reasonable that at an NS interface, superconductive properties can "leak" into the normal material [25]. This is known as the superconducting proximity effect. In this section, we will briefly discuss the NS interface by introducing Andreev reflection and then consider the situation when a quantum dot is proximal to the superconductor.

II.3.1 Andreev reflection

Consider an electron with energy E in a normal material heading towards an NS interface, see Fig. II.2. If the energy is larger than the gap of the superconductor, there are available quasiparticle states and the electron can pass the interface. If $E < \Delta$, no states are available, and the electron cannot continue into the superconductor. However, the superconductor can accept Cooper pairs at the Fermi energy. Through a process called Andreev reflection [30], the incoming electron can be reflected as a hole. The difference in charge of $2e$ before and after the Andreev reflection, which seemingly is missing from the system, has been injected into the superconductor as a Cooper pair, see Fig. II.2. This process can also happen in reverse, where a Cooper pair is transferred from the superconductor to the normal material.

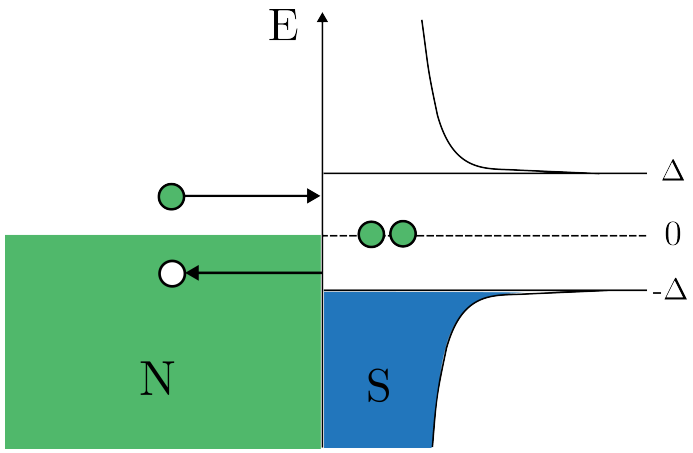

Figure II.2: An NS interface with the normal state to the left and the superconductor to the right. An electron with energy $E < \Delta$ can be Andreev reflected as a hole, resulting in the injection of a Cooper pair into the superconductor.

II.3.2 Proximity effect in quantum dots

Now, let's consider the situation when the normal material consists of a quantum dot. In Fig. II.3 below, a quantum dot is coupled to a superconductor with a tunneling amplitude t. According to the proximity effect, we expect that the properties of the superconductor will "leak" into the quantum dot.

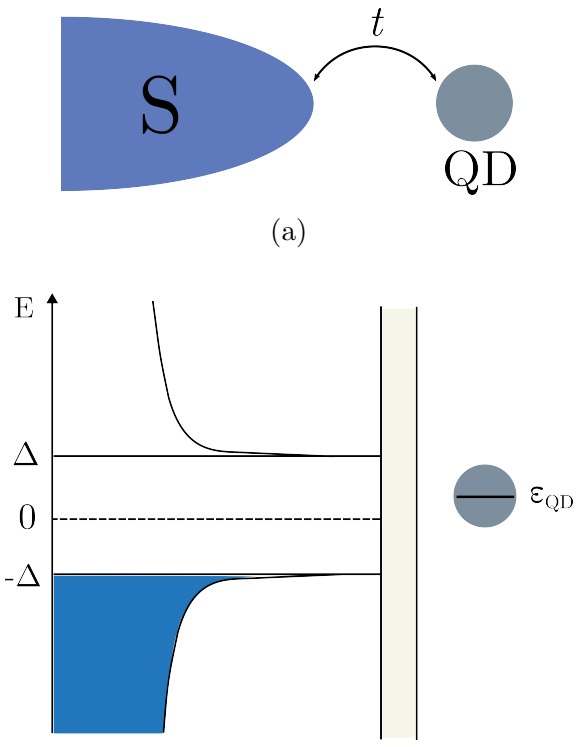

Figure II.3: A quantum dot (QD) coupled to a superconductor (S) with a tunneling amplitude t. Due to the superconducting proximity effect, the quantum dot will inherit properties of the superconductor. a) Spatial sketch of the quantum dot coupled to a superconductor. b) The density of states picture of the same system, where ϵ_{QD} is the discrete energy level of the quantum dot.

To show this, we model the system by a superconducting Anderson Hamiltonian, which originated from modeling impurities in superconductors [31]. Here, the impurity instead consists of a quantum dot. The superconducting Anderson Hamiltonian is given by

$$H = H_{\mathrm{SC}} + H_{\mathrm{QD}} + H_{\mathrm{T}}, \tag{II.18}$$

where H_{SC} is the mean-field superconducting Hamiltonian given in Eq. (II.5) and

$$H_{\mathrm{QD}} = \sum_s \epsilon_{\mathrm{QD}} d_s^\dagger d_s + U d_\uparrow^\dagger d_\uparrow d_\downarrow^\dagger d_\downarrow, \quad \text{and} \tag{II.19a}$$

$$H_{\mathrm{T}} = \sum_{\boldsymbol{k}s} t(c_{\boldsymbol{k}s}^\dagger d_s + d_s^\dagger c_{\boldsymbol{k}s}) \tag{II.19b}$$

are the quantum dot and tunneling Hamiltonians, respectively. Here, d_s annihilates a spin-s electron on the quantum dot, and $c_{\boldsymbol{k}s}$ annihilates an electron in the superconductor with momentum $\boldsymbol{k}$ and spin s. The constants ϵ_{QD} and U describe the energy level and Coulomb interaction on the quantum dot. Furthermore, the tunneling amplitude is assumed to be related to the tunneling rate by $\Gamma = 2\pi t^2 \rho_0$. The density of states the superconductor would have had in its normal state, denoted by ρ_0, is assumed to be constant.

In the limit of a large superconducting gap, i.e., $\Delta \to \infty$, one can derive an effective Hamiltonian of the proximitized quantum dot [32]. Using the method of Green's functions, the superconductor can be integrated out, resulting in an effective dot-local Hamiltonian

$$H_{\text{eff}} = \sum_s \epsilon_{\text{QD}} d_s^\dagger d_s + U d_\uparrow^\dagger d_\uparrow d_\downarrow^\dagger d_\downarrow - \Gamma(d_\uparrow^\dagger d_\downarrow^\dagger + d_\downarrow d_\uparrow). \tag{II.20}$$

Comparing with H_{QD} from Eq. (II.19), it is clear that an effective BCS-like pairing term proportional to Γ has been induced due to the coupling to the superconductor. This term can be understood as the electrons Andreev reflecting between the superconductor and the quantum dot, where two electrons can simultaneously enter or leave the quantum dot. In Appendix A.1, we further analyze the Hamiltonian in Eq. (II.20) and the formation of Andreev bound states.

When we introduce the Hamiltonian of our system in Chapter III, we include the superconducting proximity effect by a term $\Delta_{\text{ind}} d_{j\uparrow}^\dagger d_{j\downarrow}^\dagger + \text{H.c.}$, where Δ_{ind} is the induced superconducting pairing amplitude. This is a reasonable approximation for energies below the superconducting gap [33]. However, Δ_{ind} is not always proportional to the tunneling rate as in Eq. (II.20), since it is bounded by the gap of the parent superconductor.

II.4 Topological superconductivity and Majorana bound states

Topological superconductivity is a fascinating state of matter which combines the notion of superconductivity and topology. Topological superconductors, just like conventional superconductors discussed in Section II.2, have an energy gap in their dispersion relation. However, it is not possible to smoothly transform the band structure of a topological superconductor into the band structure of a normal superconductor without closing and reopening this energy gap [6, 7, 29], hence the term "topological" superconductivity.

At the boundaries and defects of topological superconductors, there is an interface between topologically trivial and nontrivial states (e.g., the vacuum). At such interfaces, there is a topology mismatch, and gapless (zero-energy) boundary states arise [29]. These are the Majorana bound states (MBSs). Majorana bound states are described by operators γ_j with the properties

$$[\gamma_j, H] = 0, \tag{II.21a}$$

$$\gamma_j^\dagger = \gamma_j, \tag{II.21b}$$

$$\{\gamma_i, \gamma_j\} = 2\delta_{ij}, \tag{II.21c}$$

where H is the Hamiltonian of the system. These properties imply that a single MBS γ_j cannot describe a creation or annihilation operator. We could try and create a

corresponding number operator $\gamma_j^\dagger \gamma_j$, however, using Eqs. (II.21b) and (II.21c), this results in $\gamma_j^\dagger \gamma_j = \gamma_j^2 = 1$, and similarly $\gamma_j \gamma_j^\dagger = 1$. An MBS is hence both empty and filled simultaneously, indicating that the occupation of an MBS is not well defined [7]. This complication is resolved by combining pairs of MBSs into fermionic operators

$$f_{ij} = \frac{1}{2}(\gamma_i + i\gamma_j), \quad f_{ij}^\dagger = \frac{1}{2}(\gamma_i - i\gamma_j), \tag{II.22}$$

which obey the fermionic commutation relations. Furthermore, we can now form number operators $n_{ij} = f_{ij}^\dagger f_{ij}$, which measures the occupancy of a pair of MBSs. For this reason, an MBS is often referred to as "half a fermion" since each fermionic state occupies two MBSs.

Since the state in Eq. (II.22) is made up of two MBSs that commute with the Hamiltonian, it takes zero energy to occupy the state. Therefore, if there are many MBSs, there is a large degenerate subspace of ground states corresponding to the occupation numbers of each pair of MBSs. In other words, the states spanned by $|n_{1,2}, n_{3,4} \ldots\rangle$, where $n_{ij} = (0, 1)$, form a subspace of degenerate ground states, which can be used to store quantum information. Furthermore, if the two MBSs making up a fermionic state are spatially separated, local perturbations cannot lift this degeneracy, and the information stored in the MBSs is protected against such perturbations.

Another exotic property of separated MBSs, due to their nonlocal nature, is nonlocal correlations and non-Abelian exchange statistics [29]. For regular (Abelian) fermions, an exchange of particles leads to a sign change, and exchanging them twice takes the system back to its original state. However, the exchange of two MBSs can rotate the wavefunction inside the degenerate subspace spanned by $|n_{1,2}, n_{3,4} \ldots\rangle$ [7]. By doing controlled exchanges of MBSs, the quantum information stored in the MBSs can be manipulated. This is the idea behind topologically protected quantum computing, one of the main motivations for studying MBSs.

In the following subsection, we introduce the simplest toy model that can host MBSs – the Kitaev chain. We also discuss how such a chain can be engineered with superconductor-semiconductor hybrid structures. Then we will introduce the notion of "poor man's MBSs" and finish by discussing how to quantify them.

II.4.1 The Kitaev chain

In 2001, Kitaev [16] proposed a famous toy model where MBSs can form, now known as the Kitaev chain. It consists of a spinless tight-binding chain with p-wave superconductivity. In contrast, the conventional superconductors described in Section II.2 are s-wave superconductors. In general, the total wave function of a Cooper pair has to be anti-symmetric since it consists of fermions. A Cooper pair in an s-wave superconductor has a symmetric spatial wavefunction, and the spin part must therefore be anti-symmetric, forming a singlet pairing between the electrons.

In a p-wave superconductor, the spatial wavefunction is anti-symmetric, and the spin part forms a symmetric triplet pairing, having the possibility to couple the same spins. For a spinless superconducting system such as the Kitaev chain, p-wave superconductivity is necessary.

The Kitaev chain Hamiltonian is given by

$$H_K = -\epsilon \sum_{j=1}^{N} c_j^\dagger c_j - \sum_{j=1}^{N-1} (t c_{j+1}^\dagger c_j + \Delta c_{j+1}^\dagger c_j^\dagger + \text{H.c.}), \tag{II.23}$$

where ϵ is the chemical potential of the chain, t is the nearest neighbor hopping amplitude, and Δ is the p-wave superconducting pairing, coupling electrons on neighboring sites. We take t and Δ to be real and positive. The following analysis of the Kitaev chain is based on the reviews in Refs. [6, 7].

Inspired by Eq. (II.22), we introduce two Majorana operators for each site j, $\gamma_{j,a}$ and $\gamma_{j,b}$. We can then rewrite the c-fermions as

$$c_j = \frac{1}{2}(\gamma_{j,b} + i\gamma_{j,a}), \quad c_j^\dagger = \frac{1}{2}(\gamma_{j,b} - i\gamma_{j,a}). \tag{II.24}$$

By rewriting the operators like this, we have split the fermion operators into two Majorana operators at the same site. Inserting the change of basis into H_K, we obtain

$$\begin{aligned} H_K = &-\frac{\epsilon}{2} \sum_{j=1}^{N} (1 + i\gamma_{j,b}\gamma_{j,a}) \\ &- \frac{i}{2} \sum_{j=1}^{N-1} [(\Delta + t)\gamma_{j,b}\gamma_{j+1,a} + (\Delta - t)\gamma_{j,a}\gamma_{j+1,b}]. \end{aligned} \tag{II.25}$$

Majorana physics becomes the most illuminating in two contrasting limits. Firstly, let's take the trivial limit $t = \Delta = 0$. Then, the second line of Eq. (II.25) disappears, and we only have couplings of Majorana operators $\gamma_{j,a}$ and $\gamma_{j,b}$ living at the same site. In this limit, there is a unique ground state consisting of the vacuum of c-operators. If we instead take the limit $\epsilon = 0$ and $t = \Delta \neq 0$, H_K reduces to

$$H_K = -it \sum_{j=1}^{N-1} \gamma_{j,b}\gamma_{j+1,a}. \tag{II.26}$$

Then, we only have coupling between Majorana operators on adjacent sites. If we now pair these Majorana operators into new fermionic operators d_j by forming $d_j = \frac{1}{2}(\gamma_{j+1,a} + i\gamma_{j,b})$, the Hamiltonian becomes

$$H_K = 2t \sum_{j=1}^{N-1} d_j^\dagger d_j. \tag{II.27}$$

At first glance, this does not seem very interesting. The Hamiltonian is diagonal in the d-operators, and it takes an energy $2t$ to add a d-particle to the system. At a

closer look, however, we see that the Majorana operators $\gamma_{1,a}$ and $\gamma_{N,b}$ located at each end of the chain are missing from Eq. (II.27). These Majorana operators can be combined into

$$f = \frac{1}{2}(\gamma_{1,a} + i\gamma_{N,b}), \tag{II.28}$$

such that the two MBSs at each end form a single fermionic mode. This is an example of the highly non-local states discussed previously in this section. Since the Majorana operators in f are missing from the Hamiltonian, they commute with H_K and it takes zero energy to occupy this state. The ground state is hence two-fold degenerate between the vacuum state $|0\rangle$ defined by $f|0\rangle = 0$, and the state where the two MBSs are occupied, defined by $|1\rangle = f^\dagger|0\rangle$. The states $|0\rangle$ and $|1\rangle$ are said to have different parity (even or odd) since they contain an even and odd number of fermions, respectively.

The two MBSs appear at the ends of the chain because they form an interface between topologically trivial and nontrivial states (vacuum). The Kitaev chain is in a topological phase as long as the chemical potential is within the gap to the excited states, i.e., $|\epsilon| < 2t$ and with a non-zero pairing amplitude $\Delta \neq 0$. However, in general, the Majorana operators are not entirely localized on the outermost sites. Instead, they decay exponentially away from the edges [6].

II.4.2 Engineering the Kitaev chain

The Kitaev chain requires spinless, p-wave superconductivity, as stated in the previous section. Unfortunately, not only do superconductors consist of spinful electrons, but p-wave superconductivity is scarce in nature. Finding a material mimicking the Kitaev chain is, therefore, difficult. However, the challenge became much more achievable when it was realized that the proximity effect in superconductor-semiconductor structures could induce p-wave superconductivity. In this way of engineering an effective Kitaev chain, the following three ingredients are required [7]:

1. Conventional (s-wave) superconductivity.

2. Strong magnetic fields to reach an effective spinless system.

3. Spin-orbit coupling (or a spatially varying magnetic field [34]).

Low-energy descriptions of systems with these ingredients can directly be mapped to the Kitaev chain. Some examples of systems that could host MBSs include one-dimensional semiconducting nanowires proximitized by superconductors [5] and chains of quantum dots separated by superconductors [35].

Despite many efforts to detect MBSs in hybrid superconductor-semiconductor structures, no conclusive evidence has yet been found. Although signatures of MBSs have been reported [9–12], there has been no way to assure that the signals do

not come from other, trivial states living at zero energy [13–15]. Furthermore, no evidence of the non-Abelian nature of MBSs has been found. Hence there has recently been a push to study simpler systems where MBSs can appear. Instead of reaching a topological phase and detecting MBSs at interfaces to trivial states, the idea has been to engineer a minimal Kitaev chain of just two sites. In such systems, poor man's MBSs are predicted to form.

II.4.3 Poor man's Majorana bound states

In 2023, experimental signatures consistent with MBSs were found in a double quantum dot system separated by a superconductor, effectively forming a two-site Kitaev chain [19]. The idea of this setup dates back to Ref. [17], where the term "poor man's" MBSs was coined. The MBSs theorized to appear in such short Kitaev chains were called "poor man's" since they lack the topological protection MBSs in topological matter offer. Instead, the poor man's MBSs appear when fine-tuning the system to sweet spots. At a sweet spot, two MBSs form, one entirely localized on the left dot and the other on the right dot. The MBSs are hence spatially separated just like the ones appearing in topological matter and could be studied for their non-Abelian exchange statistics.

A generalized version of the Kitaev chain in Eq. (II.23) is given by

$$H_K = \sum_{j=1}^{N} \epsilon_j c_j^\dagger c_j + \sum_{j=1}^{N-1} (t_j e^{i\Theta_j} c_{j+1}^\dagger c_j + \Delta_j e^{i\Phi_j} c_{j+1}^\dagger c_j^\dagger + \text{H.c.}), \tag{II.29}$$

where the parameters can now vary along the chain. Furthermore, the phases of the tunneling and superconducting pairing are now included. It can be shown that a sweet spot where two MBSs are localized entirely on each end of the chain can be found when

$$\epsilon_j = 0, \tag{II.30a}$$
$$t_j = \Delta_j, \tag{II.30b}$$

forming an energy gap to the next excited state by $E_{\text{gap}} = 2\min\{t_j\}$ [1]. These conditions define the sweet spot to which one must tune the system to find MBSs at each end of the chain. In the simplified Kitaev chain analyzed at the beginning of this chapter, we showed that in the limit of Eq. (II.30), two Majorana operators disappeared from the Hamiltonian and formed MBSs at each end of the chain.

In the original poor man's model [17], the two-site Kitaev chain emerges from considering an infinite magnetic field that fully spin-polarizes the dots. This reduces the Hilbert space significantly and allows for analytical results. However, in practice, the strength of the magnetic field is bounded by the fact that large magnetic fields destroy superconductivity [2]. Therefore, the analysis of a poor man's system in

Ref. [18] considers a finite magnetic field and spinful quantum dots. Furthermore, intra-dot Coulomb interactions were also considered. However, two issues appear when considering finite magnetic fields and Coulomb interactions. Firstly, a perfect sweet spot might not exist since the system does not directly map to the Kitaev chain. Secondly, the conditions for the "best" sweet spot are not necessarily given by Eq. (II.30) anymore. Therefore, a quality measure of the MBSs appearing in the poor man's systems is necessary to resolve these issues. By forming a loss function based on relevant quality measures of the MBSs, numerical optimization allows for locating the best sweet spot. The MBS quality can then be evaluated at this optimized sweet spot.

II.4.4 Quantifying Majorana bound states

To quantify MBSs appearing in the short Kitaev chains, one can take inspiration from "perfect" MBSs in the topological phase and use their properties as a quality measure. During the work of the thesis, two quality measures have been developed and used: the energy degeneracy and the local distinguishability between the odd and even ground states.

Energy degeneracy

The first quality measure is the energy difference between the odd and even ground states. As the MBSs are zero-energy excitations, the odd and even ground states should be degenerate at a perfect sweet spot. To quantify this, we have constructed an energy degeneracy quality measure defined as

$$\delta E = \frac{E_{\text{odd}} - E_{\text{even}}}{E_{\text{gap}}}, \tag{II.31}$$

where $E_{\text{gap}} = E_{\text{exc}} - \max\{E_{\text{odd}}, E_{\text{even}}\}$ is the minimal energy difference between the ground states and the next excited state. At a perfect sweet spot, $\delta E = 0$. However, this is not a sufficient condition, so other complementary quality measures must be used.

Local distinguishability

Another property of the Kitaev chain in its topological phase is that measurements done locally cannot reveal if the system is in its odd or even ground state – the two ground states are locally indistinguishable. To quantify this property, we define local distinguishability (LD) as

$$\text{LD} = \frac{1}{N}\sum_{j=1}^{N} \|\rho_j^o - \rho_j^e\| = \frac{1}{N}\sum_{j=1}^{N} \|\delta\rho_j\|, \tag{II.32}$$

which is zero at a perfect sweet spot. We will later show that the LD is related to how protected the ground state degeneracy is against local perturbations. In Eq. (II.32), $\|\cdot\|$ is the Frobenius norm, N is the number of sites in the system and ρ_j^η is the reduced density matrix at site j for the odd ($\eta = o$) or even ($\eta = e$) ground state. The reduced density matrix is a way to describe a quantum state as seen by looking only at a subsystem of the full system. The difference between reduced density matrices of the odd and even ground state is, therefore, a natural measure of how distinguishable the states are when probing locally.

Due to quantum entanglement, information of the full state is lost when only looking at parts of the system. From an observer's perspective, only looking locally at a subsystem, the quantum state is in a statistical mixture of different states. The reduced density matrix is defined in a way to ensure that the expectation value of a local measurement on the subsystem is the same when using the reduced density matrix or the full quantum state to calculate it [36]. Using this property, we can show that the LD gives an estimate of how protected the ground state degeneracy is against local perturbations.

Consider a perturbation V_R, local to the region R. In first-order perturbation theory, the energy perturbation E_p^η on the η-parity ground state is

$$\langle E_p^\eta \rangle = \langle \eta | V_\mathrm{R} | \eta \rangle = \mathrm{Tr}\,(\rho^\eta V_\mathrm{R}) = \mathrm{Tr}\,(\rho_\mathrm{R}^\eta V_\mathrm{R}), \tag{II.33}$$

where ρ^η is the full density matrix of the η-parity state. In the final equality, we have used the above-mentioned defining property of the reduced density matrix. Using Eq. (II.33), we can look at the difference between the change in energy of the odd and even ground states due to the perturbation V_R:

$$\langle \Delta E \rangle = \langle E_p^o \rangle - \langle E_p^e \rangle = \mathrm{Tr}\,(\rho_\mathrm{R}^o V_\mathrm{R}) - \mathrm{Tr}\,(\rho_\mathrm{R}^e V_\mathrm{R}) = \mathrm{Tr}\,(\delta\rho_\mathrm{R} V_\mathrm{R}) = (\delta\rho_\mathrm{R}, V_\mathrm{R}), \tag{II.34}$$

where $(\cdot,\cdot)$ is the Frobenius inner product. If the odd and even states were degenerate to begin with, i.e., if $\delta E = 0$, $\langle \Delta E \rangle$ is an estimate of the energy splitting between the states due to V_R. Using the Cauchy-Schwartz inequality, we get

$$|\langle \Delta E \rangle| = |(\delta\rho_\mathrm{R}, V_\mathrm{R})| \leq \|\delta\rho_\mathrm{R}\| \|V_\mathrm{R}\| \implies \frac{|\langle \Delta E \rangle|}{\|V_\mathrm{R}\|} \leq \|\delta\rho_\mathrm{R}\|. \tag{II.35}$$

Thus, $\|\delta\rho_\mathrm{R}\|$ is an upper bound to the ratio between the first-order energy splitting due to V_R and the strength of V_R. The LD in Eq. (II.32) is an average of this bound for perturbations at each site in the system and therefore quantifies how protected the system is against local perturbations in general. This ties back to the properties of MBSs discussed in Section II.4, where it was said that spatially separate MBSs are robust against local perturbations.

Based on the two quality measures, we define a loss function

$$\mathrm{Loss} = \delta E^2 + \mathrm{LD}^2 \tag{II.36}$$

which we want to minimize to find the best sweet spot. For more details of the optimization procedure, see Section IV.1.

III

The model and its Kitaev limit

In this chapter, we begin by presenting the model and Hamiltonian of the chain of interacting quantum dots proximitized by superconductors. Most of the modeling is based on Ref. [37], where a similar system is analyzed. Starting out with a rather general Hamiltonian in Eqs. (III.1) and (III.2), we will then perform an operator transformation to simplify parts of the Hamiltonian. Next, we invoke a few assumptions and go through a short derivation, after which the final form of the Hamiltonian in Eq. (III.9) is obtained. In the second section of this chapter, we go through the derivation sketched in Ref. [1], which shows that the system (without interactions) maps to the Kitaev chain for large magnetic fields. The main result is Eq. (III.23), where the effective Kitaev parameters are presented.

III.1 Model: Chain of interacting quantum dots proximitized by superconductors

In this thesis, we consider a chain of interacting quantum dots, where each dot is proximitized by a superconductor. Furthermore, non-colinear magnetic fields are applied at each dot. However, the rotation of the magnetic fields can be replaced by spin-orbit coupling. We will consider chain lengths between two and four sites. For a sketch of the system, see Fig. III.1.

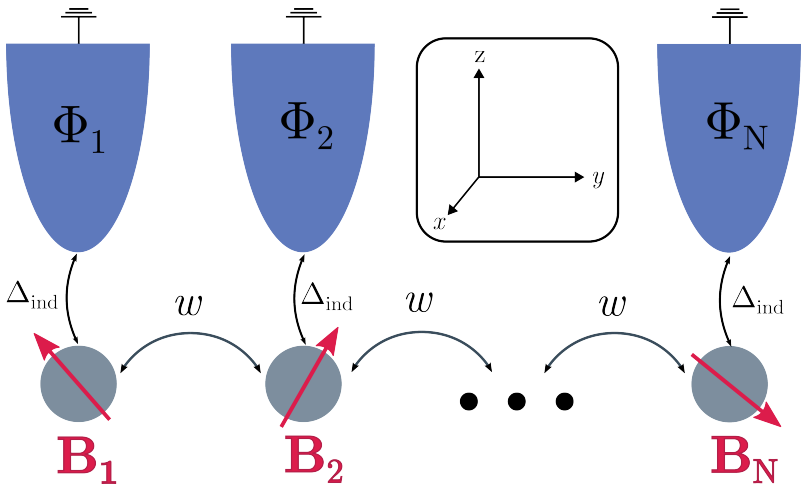

Figure III.1: Sketch of the quantum dot chain with N sites. The tunneling amplitude between the quantum dots is homogenous and given by w. At each quantum dot, a superconductor with phase ϕ_j induces a superconducting pairing term on the dot with amplitude Δ_{ind}. Finally, non-colinear magnetic fields $\boldsymbol{B}_j$ are applied at each dot.

We model the system by the following Hamiltonian:

$$H = H_{\text{QD}} + H_t + H_{\text{mag}} + H_{\text{ind}}, \tag{III.1}$$

where H_{QD} includes the chemical potential on each quantum dot and Coulomb interactions, H_t is the tunneling Hamiltonian, H_{mag} contains the contributions from the magnetic fields, and H_{ind} includes the induced superconductivity from the proximity effect. Each term is given by

$$H_{\text{QD}} = \mu \sum_{j,s} n_{js} + U_{\text{intra}} \sum_{j} n_{j\uparrow} n_{j\downarrow} + U_{\text{inter}} \sum_{j} N_j N_{j+1}, \tag{III.2a}$$

$$H_t = w \sum_{j,s} d^\dagger_{j,s} d_{j+1,s} + \text{H.c.}, \tag{III.2b}$$

$$H_{\text{mag}} = \sum_{j,s,s'} \frac{1}{2} g\mu_B (\boldsymbol{B}_j \cdot \boldsymbol{\sigma})_{ss'} d^\dagger_{js} d_{js'}, \tag{III.2c}$$

$$H_{\text{ind}} = \Delta_{\text{ind}} \sum_{j} e^{i\phi_j} d^\dagger_{j\uparrow} d^\dagger_{j\downarrow} + \text{H.c.}. \tag{III.2d}$$

Here, d_{js} annihilates a spin-s electron (measured along the z-axis) on site j and $n_{js} = d^\dagger_{js} d_{js}$ is the corresponding number operator. Furthermore, $N_j = n_{j\uparrow} + n_{j\downarrow}$ is the operator for the total number of electrons on each site. The parameters we consider fixed along the chain are the chemical potential μ of the quantum dots, the intra-dot and inter-dot Coulomb interactions U_{intra} and U_{inter}, the real and positive tunneling amplitude w, and the absolute value of the induced superconducting pairing Δ_{ind}. However, the phase of the induced pairing ϕ_j can vary along the chain. The magnetic field at site j is given by $\boldsymbol{B}_j = B_0 \hat{\boldsymbol{b}}_j$, where B_0 is the magnitude of the magnetic

field, taken to be constant along the chain, and $\hat{\boldsymbol{b}}_j$ is the direction of the magnetic field, which varies with j. We denote the Zeeman energy with $V_z = g\mu_B B_0/2$, where g is the Landé g-factor and μ_B the Bohr magneton. Furthermore, $\boldsymbol{\sigma} = (\sigma_x, \sigma_y, \sigma_z)$ is the vector of Pauli matrices, and hence $(\boldsymbol{B}_j \cdot \boldsymbol{\sigma})_{ss'} = B_0(b_j^x\sigma_x + b_j^y\sigma_y + b_j^z\sigma_z)_{ss'}$, where the index ss' indicates the matrix element between spins s and s'.

Following Ref. [37], we align the spin basis with the magnetic field direction at each site, which in polar coordinates is given by $\hat{\boldsymbol{b}}_j = (\sin\theta_j\cos\varphi_j, \sin\theta_j\sin\varphi_j, \cos\theta_j)$. This way, the spin is measured in the same direction as the magnetic field. We perform a SU(2) transformation of the operators given by

$$\begin{pmatrix} d_{j\uparrow} \\ d_{j\downarrow} \end{pmatrix} = U_j \begin{pmatrix} \tilde{d}_{j\uparrow} \\ \tilde{d}_{j\downarrow} \end{pmatrix}, \tag{III.3}$$

where $\tilde{d}_{js}$ are the new, rotated operators and

$$U_j = \begin{pmatrix} \cos(\theta_j/2) & -\sin(\theta_j/2)e^{-i\varphi_j} \\ \sin(\theta_j/2)e^{i\varphi_j} & \cos(\theta_j/2) \end{pmatrix}. \tag{III.4}$$

Applying the transformation, the terms of the Hamiltonian in Eq. (III.2) transform into

$$H_{\text{QD}} = \mu\sum_{j,s}\tilde{n}_{js} + U_{\text{intra}}\sum_j \tilde{n}_{j\uparrow}\tilde{n}_{j\downarrow} + U_{\text{inter}}\sum_j \tilde{N}_j\tilde{N}_{j+1}, \tag{III.5a}$$

$$H_t = w\sum_{j,ss'}\Omega_{j,ss'}\tilde{d}^\dagger_{j,s}\tilde{d}_{j+1,s'} + \text{H.c.}, \tag{III.5b}$$

$$H_{\text{mag}} = \sum_{j,s,s'} V_z\sigma_{z,ss'}\tilde{d}^\dagger_{js}\tilde{d}_{js'} = \sum_j V_z(\tilde{n}_{j\uparrow} - \tilde{n}_{j\downarrow}), \tag{III.5c}$$

$$H_{\text{ind}} = \Delta_{\text{ind}}\sum_j e^{i\Phi_j}\tilde{d}^\dagger_{j\uparrow}\tilde{d}^\dagger_{j\downarrow} + \text{H.c.}. \tag{III.5d}$$

where $\Omega_j = U_j^\dagger U_{j+1}$ which evaluates to

$$\Omega_j = \begin{pmatrix} \alpha_j & -\beta_j \\ \beta_j & \alpha_j^* \end{pmatrix}, \tag{III.6a}$$

$$\alpha_j = \cos\frac{\theta_j}{2}\cos\frac{\theta_{j+1}}{2} + \sin\frac{\theta_j}{2}\sin\frac{\theta_{j+1}}{2}e^{-i(\varphi_j-\varphi_{j+1})}, \tag{III.6b}$$

$$\beta_j = -\sin\frac{\theta_j}{2}\cos\frac{\theta_{j+1}}{2}e^{i\varphi_j} + \cos\frac{\theta_j}{2}\sin\frac{\theta_{j+1}}{2}e^{i\varphi_{j+1}}. \tag{III.6c}$$

The transformation from Eq. (III.2) to Eq. (III.5) has simplified H_{mag} since the magnetic field is now aligned with the spin basis at each dot. The difficulty now lies in the tunneling term H_t.

Next, we consider a couple of simplifying assumptions. Firstly, we take $\varphi_j = \varphi$ to be constant, such that the rotation of the magnetic field lies in a single plane (perpendicular to the xy-plane) along the chain. Furthermore, we assume that the

magnetic field's rotation between two sites is the same everywhere, i.e., $\delta\theta_j = \theta_{j+1} - \theta_j = \delta\theta$. Using these assumptions, $\alpha_j = \alpha = \cos(\delta\theta/2)$ and $\beta_j = \beta = \sin(\delta\theta/2)e^{i\varphi}$ become site-independent and $\Omega_j = \Omega$ reduces to

$$\Omega = \begin{pmatrix} \cos(\delta\theta/2) & -\sin(\delta\theta/2)e^{i\varphi} \\ \sin(\delta\theta/2)e^{-i\varphi} & \cos(\delta\theta/2) \end{pmatrix}. \tag{III.7}$$

By inserting Ω in Eq. (III.5), the tunneling Hamiltonian simplifies to

$$H_t = w\cos\frac{\delta\theta}{2}\sum_{js}\tilde{d}^\dagger_{js}\tilde{d}_{j+1,s} + w\sin\frac{\delta\theta}{2}\sum_j(e^{i\varphi}\tilde{d}^\dagger_{j\downarrow}\tilde{d}_{j+1,\uparrow} - e^{-i\varphi}\tilde{d}^\dagger_{j\uparrow}\tilde{d}_{j+1,\downarrow}) + \text{H.c.} \tag{III.8}$$

The first term represents tunneling between spins that are either both parallel or both anti-parallel to the magnetic fields at the corresponding site. This term is proportional to $w\cos(\delta\theta/2)$ and hence disappears if the magnetic fields on neighboring dots are anti-parallel ($\delta\theta = \pi$). The second term in H_t represents tunneling between sites where one spin is parallel and the other is anti-parallel to the magnetic fields. Since this term is proportional to $w\sin(\delta\theta/2)$, it disappears when there is no magnetic field rotation.

For completeness, we write the final form of the total Hamiltonian for the interacting quantum dot chain as

$$\begin{aligned} H = &\sum_{j,s}(\mu + \eta_s V_z)\tilde{n}_{js} + U_{\text{intra}}\sum_j \tilde{n}_{j\uparrow}\tilde{n}_{j\downarrow} + U_{\text{inter}}\sum_j \tilde{N}_j\tilde{N}_{j+1} \\ &+ w\cos\frac{\delta\theta}{2}\sum_{js}[\tilde{d}^\dagger_{js}\tilde{d}_{j+1,s} + \text{H.c.}] \\ &+ w\sin\frac{\delta\theta}{2}\sum_j[\tilde{d}^\dagger_{j\downarrow}\tilde{d}_{j+1,\uparrow} - \tilde{d}^\dagger_{j\uparrow}\tilde{d}_{j+1,\downarrow} + \text{H.c.}] \\ &+ \Delta_{\text{ind}}\sum_j[e^{i\phi_j}\tilde{d}^\dagger_{j\uparrow}\tilde{d}^\dagger_{j\downarrow} + \text{H.c.}], \end{aligned} \tag{III.9}$$

where $\eta_\uparrow = 1$ and $\eta_\downarrow = -1$ and we have set $\varphi = 0$. This is the form of the Hamiltonian we will study analytically and numerically in the remainder of this work.

III.2 The Kitaev limit without interactions

In Ref. [1], it is shown that the Hamiltonian in Eq. (III.9) without interactions maps to the Kitaev chain (see Eq. (II.29)) for large Zeeman energies in comparison to the tunneling amplitude. This is not obvious for a couple of reasons. Firstly, the Kitaev chain requires a non-local superconducting pairing of the form $c^\dagger_{j+1}c^\dagger_j$, while, in our Hamiltonian, we only have the local superconducting pairing $\tilde{d}^\dagger_{j\uparrow}\tilde{d}^\dagger_{j\downarrow}$. However, an effective non-local pairing can be formed by the following two-step process: 1) An

Andreev reflection of a Cooper pair from the superconductor to one quantum dot, followed by 2) tunneling of one of the Cooper paired electrons to the neighboring dot. The process is sketched in Fig. III.2.

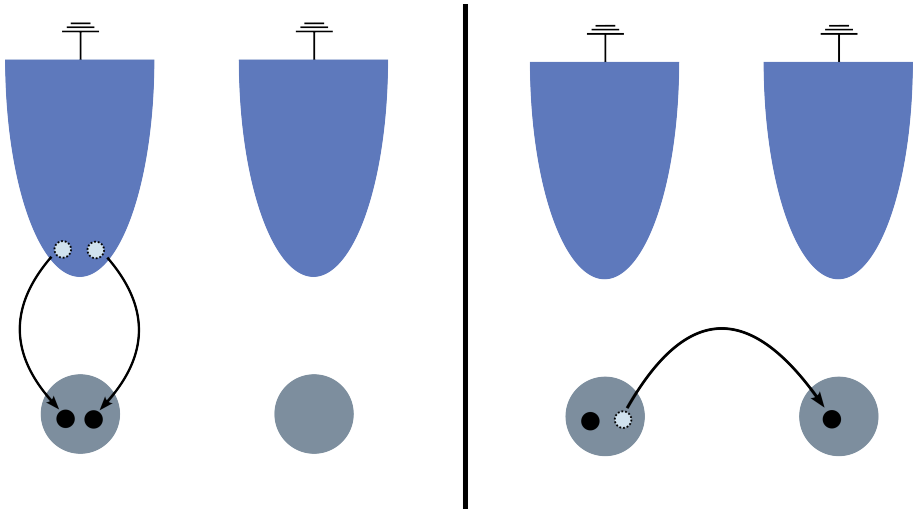

Figure III.2: Firstly, two electrons Andreev reflect onto one of the quantum dots (left). Then, one of the electrons tunnels to the other dot (right). This creates effective non-local superconducting pairing between neighboring sites in the quantum dot chain.

Secondly, as discussed in Section II.4.2, to engineer a Kitaev chain, a strong magnetic field is required to turn the system spinless at low energies. However, since the local superconducting pairing results in both spins occupying the quantum dots to some extent, it seems like we have destroyed the spinless feature of the system. Yet, Ref. [1] showed that in the limit of a large magnetic field, the chain indeed only consists of one particle species. The trick is that the species is not one of the spin-up or spin-down operators but as quasiparticles consisting of superpositions of particles and holes. In the rest of this section, we will go through this derivation.

We start by looking at the local Hamiltonian for an isolated, single quantum dot at site j in the chain, assuming no interactions:

$$H_j = \sum_s (\mu + \eta_s V_z)\tilde{n}_{js} + \Delta_{\text{ind}}[e^{i\phi_j}\tilde{d}^\dagger_{j\uparrow}\tilde{d}^\dagger_{j\downarrow} + \text{H.c.}]. \tag{III.10}$$

Since the Hamiltonian in Eq. (III.10) is quadratic, we can use the BdG formalism to find new quasiparticle operators which diagonalize H_j. Following the method described in Section II.2.3, we introduce the vector of operators $\Psi_j = (\tilde{d}_{j\uparrow}, \tilde{d}_{j\downarrow}, \tilde{d}^\dagger_{j\uparrow}, \tilde{d}^\dagger_{j\downarrow})^T$ and rewrite H_j as

$$H_j = \frac{1}{2}\Psi_j^\dagger h_j \Psi_j + \mu, \tag{III.11}$$

with the BdG Hamiltonian

$$h_j = \begin{pmatrix} \mu + V_z & 0 & 0 & \Delta_{\text{ind}} e^{i\phi_j} \\ 0 & \mu - V_z & -\Delta_{\text{ind}} e^{i\phi_j} & 0 \\ 0 & -\Delta_{\text{ind}} e^{-i\phi_j} & -(\mu + V_z) & 0 \\ \Delta_{\text{ind}} e^{-i\phi_j} & 0 & 0 & -(\mu - V_z) \end{pmatrix}. \tag{III.12}$$

We then solve the BdG equations

$$h_j \psi = E\psi, \tag{III.13}$$

where $\psi = (u_\uparrow, u_\downarrow, v_\uparrow, v_\downarrow)^T$, and get the energies $E = \pm(V_z \pm \sqrt{\mu^2 + \Delta_{\text{ind}}^2})$. Because of particle-hole symmetry (see Section II.2.3), we can restrict ourselves to the positive energy solutions, which we can assume to be given by $\pm V_z + \sqrt{\mu^2 + \Delta_{\text{ind}}^2}$. The corresponding eigenvectors are

$$\begin{aligned} \psi_b &= \frac{e^{-i\phi_j/2}}{\sqrt{2\beta}} \begin{pmatrix} e^{i\phi_j}\sqrt{\beta+\mu} & 0 & 0 & \sqrt{\beta-\mu} \end{pmatrix}^T, \quad E_b = V_z + \beta, \\ \psi_a &= \frac{e^{-i\phi_j/2}}{\sqrt{2\beta}} \begin{pmatrix} 0 & -e^{i\phi_j}\sqrt{\beta+\mu} & \sqrt{\beta-\mu} & 0 \end{pmatrix}^T, \quad E_a = -V_z + \beta, \end{aligned} \tag{III.14}$$

where $\beta = \sqrt{\mu^2 + \Delta_{\text{ind}}^2}$. Using particle-hole symmetry, we can form the two remaining eigenvectors and construct the transformation matrix

$$\Gamma_j = \frac{e^{-i\phi_j/2}}{\sqrt{2\beta}} \begin{pmatrix} e^{i\phi_j}\sqrt{\beta+\mu} & 0 & 0 & e^{i\phi_j}\sqrt{\beta-\mu} \\ 0 & -e^{i\phi_j}\sqrt{\beta+\mu} & e^{i\phi_j}\sqrt{\beta-\mu} & 0 \\ 0 & \sqrt{\beta-\mu} & \sqrt{\beta+\mu} & 0 \\ \sqrt{\beta-\mu} & 0 & 0 & -\sqrt{\beta+\mu} \end{pmatrix}. \tag{III.15}$$

Finally, we can find the new operators $\Xi_j = (b_j, a_j, b_j^\dagger, a_j^\dagger)^T$ by forming

$$\Xi_j = \Gamma_j^\dagger \Psi_j. \tag{III.16}$$

For the annihilation operators, we get

$$\begin{aligned} a_j &= \frac{e^{i\phi_j/2}}{\sqrt{2\beta}} \left(\sqrt{\beta-\mu}\ \tilde{d}_{j\uparrow}^\dagger - e^{-i\phi_j}\sqrt{\beta+\mu}\ \tilde{d}_{j\downarrow} \right), \\ b_j &= \frac{e^{i\phi_j/2}}{\sqrt{2\beta}} \left(\sqrt{\beta-\mu}\ \tilde{d}_{j\downarrow}^\dagger + e^{-i\phi_j}\sqrt{\beta+\mu}\ \tilde{d}_{j\uparrow} \right). \end{aligned} \tag{III.17}$$

These are the quasiparticle operators that diagonalize H_j, meaning that

$$H_j = (\beta + V_z) b_j^\dagger b_j + (\beta - V_z) a_j^\dagger a_j, \tag{III.18}$$

where the constant term is, as usually, neglected.

The idea of Boguliobov transforming the local Hamiltonian is to express the original $\tilde{d}$ operators in terms of the new a and b operators. This is done by inverting Eq. (III.16)

$$\Psi_j = \begin{pmatrix} \tilde{d}_{j\uparrow} \\ \tilde{d}_{j\downarrow} \\ \tilde{d}^\dagger_{j\uparrow} \\ \tilde{d}^\dagger_{j\downarrow} \end{pmatrix} = \Gamma_j \Xi_j = \frac{1}{\sqrt{2\beta}} \begin{pmatrix} e^{i\phi_j/2}(\sqrt{\beta-\mu}\; a^\dagger_j + \sqrt{\beta+\mu}\; b_j) \\ e^{i\phi_j/2}(\sqrt{\beta-\mu}\; b^\dagger_j - \sqrt{\beta+\mu}\; a_j) \\ e^{-i\phi_j/2}(\sqrt{\beta-\mu}\; a_j + \sqrt{\beta+\mu}\; b^\dagger_j) \\ e^{-i\phi_j/2}(\sqrt{\beta-\mu}\; b_j - \sqrt{\beta+\mu}\; a^\dagger_j) \end{pmatrix}. \tag{III.19}$$

Equipped with the expressions in Eq. (III.19), we can return to the full Hamiltonian in Eq. (III.9). Without interactions, we write it as

$$H' = \sum_j H_j + H_t = \sum_j (\beta + V_z) b^\dagger_j b_j + (\beta - V_z) a^\dagger_j a_j + H_t, \tag{III.20}$$

where H_t is the tunneling Hamiltonian given in Eq. (III.8) with $\varphi = 0$. If we have a large Zeeman energy, the b particles will live at much larger energies than the a particles. If we further assume that the tunneling amplitude w is much smaller than the Zeeman energy, $w \ll V_z$, the occupancy of the b-excitations will be negligible for the low energy states of the system. Hence, we can safely project H' onto the states without b-excitations by throwing away terms that include b operators. However, note that terms of the form $bb^\dagger$, which count the number of b-quasiholes, evaluate to one in this approximation since the level is always empty.

Using Eq. (III.19), we can express H_t in terms of a and b operators and project it by only keeping the terms with a operators. We get

$$\begin{aligned} \tilde{d}^\dagger_{j\uparrow}\tilde{d}_{j+1,\uparrow} + \text{H.c.} &\to -\frac{e^{-i\delta\phi_j/2}}{2\beta}(\beta-\mu) a^\dagger_{j+1} a_j + \text{H.c.}, \\ \tilde{d}^\dagger_{j\downarrow}\tilde{d}_{j+1,\downarrow} + \text{H.c.} &\to \frac{e^{-i\delta\phi_j/2}}{2\beta}(\beta+\mu) a^\dagger_j a_{j+1} + \text{H.c.}, \\ \tilde{d}^\dagger_{j\downarrow}\tilde{d}_{j+1,\uparrow} + \text{H.c.} &\to \frac{e^{-i\delta\phi_j/2}}{2\beta}\Delta_{\text{ind}} a^\dagger_{j+1} a^\dagger_j + \text{H.c.}, \\ -\tilde{d}^\dagger_{j\uparrow}\tilde{d}_{j+1,\downarrow} + \text{H.c.} &\to \frac{e^{-i\delta\phi_j/2}}{2\beta}\Delta_{\text{ind}} a_j a_{j+1} + \text{H.c.}, \end{aligned} \tag{III.21}$$

where $\delta\phi_j = \phi_j - \phi_{j+1}$ is the superconducting phase difference between two sites. From this projection, we get two different kinds of terms. One corresponds to normal tunneling of the form $a^\dagger_{j+1}a_j$, and the other corresponds to a non-local pairing of the form $a^\dagger_{j+1}a^\dagger_j$. Inserting Eq. (III.21) into the tunneling Hamiltonian H_t, we get

$$\begin{aligned} H' = \sum_j (\beta - V_z) a^\dagger_j a_j + \sum_j \Bigg[& w \cos\frac{\delta\theta}{2}\left(\frac{\mu}{\beta}\cos\frac{\delta\phi_j}{2} + i\sin\frac{\delta\phi_j}{2}\right) a^\dagger_{j+1} a_j \\ & + \frac{w\Delta_{\text{ind}}}{\beta}\sin\frac{\delta\theta}{2}\cos\frac{\delta\phi_j}{2} a^\dagger_{j+1} a^\dagger_j + \text{H.c.}\Bigg] \end{aligned} \tag{III.22}$$

Comparing with Eq. (II.23), we see that H' maps to the Kitaev chain in the a operators with the following effective parameters

$$\epsilon = \beta - V_z = \sqrt{\mu^2 + \Delta_{\text{ind}}^2} - V_z, \tag{III.23a}$$

$$te^{i\Theta} = w \cos\frac{\delta\theta}{2}\left(\frac{\mu}{\beta}\cos\frac{\delta\phi}{2} + i\sin\frac{\delta\phi}{2}\right), \tag{III.23b}$$

$$\Delta e^{i\Phi} = \frac{w\Delta_{\text{ind}}}{\beta}\sin\frac{\delta\theta}{2}\cos\frac{\delta\phi}{2}. \tag{III.23c}$$

To have completely site-independent Kitaev-parameters, we have chosen $\delta\phi_j = \delta\phi$ to be constant.

IV

Methodology

The computational work of the thesis involves numerically implementing and diagonalizing the Hamiltonian in Eq. (III.9) to calculate the eigenstates and eigenenergies of the interacting quantum dot chain. In particular, the ground states in each parity sector are of interest. The ground states in the odd and even parity sectors and their corresponding energies are used to numerically evaluate the quality measures defined in Section II.4.4. Finally, we evaluate the loss function in Eq. (II.36). The loss function is then optimized to find the parameters corresponding to the sweet spot. See Section IV.1 for more details about the optimization procedure. A corresponding routine for calculating the quality measures and optimizing for the sweet spot in the Kitaev chain is also implemented.

The programming language of choice is Julia [38]. In particular, we use the `QuantumDots.jl` package [39], which has been implemented by one of the supervisors of this thesis. To perform the numerical optimization of the loss function, we use the `BlackBoxOptim.jl` package [40]. Furthermore, in Ref. [41], the computational routines written by the author can be found, such as the implementation of the interacting quantum dot chain Hamiltonian, the quality measures, and the optimization procedure.

IV.1 Optimization procedure

To find the best sweet spot, we optimize the loss function in Eq. (II.36) based on the two quality measures defined in Section II.4.4. For the interacting quantum dot chain, we optimize the parameters in the $(\Delta_{\text{ind}}/w, \mu/w)$-plane, fixing all other parameters. The initial guess for the optimization procedure $(\Delta_{\text{ind,init}}/w, \mu_{\text{init}}/w)$ is based on the Kitaev limit (large Zeeman energies), where we know the location of the sweet spot; see Eqs. (V.8) and (V.9) in the next chapter. Furthermore, the region for optimization has been determined through a trial and error process to ensure

that the sweet spot is inside the region. The resulting range for each parameter is given by $\Delta_{\text{ind}} = (0, \Delta_{\text{ind,init}} + \delta\Delta_{\text{ind}})$ and $\mu = (\mu_{\text{init}} - \delta\mu, \mu_{\text{init}} + \delta\mu)$, where

$$\delta\mu = \max\{2V_z + 2U_{\text{inter}} + \frac{1}{2}U_{\text{intra}}, 2w\}, \tag{IV.1a}$$

$$\delta\Delta_{\text{ind}} = \max\{V_z + U_{\text{inter}} + \frac{1}{2}U_{\text{intra}}, 2w\}. \tag{IV.1b}$$

The maximum function ensures that $\delta\Delta_{\text{ind}}, \delta\mu \geq 2w$. Otherwise, if setting $\delta\Delta_{\text{ind}}$ and $\delta\mu$ to the first argument in the maximum functions in Eq. (IV.1), the optimization region would become too small without interactions and with a small Zeeman energy.

To compare the quality of sweet spots for different configurations, we want to fix one of the quality measures (δE) at a small value and optimize the second (LD). To do this, we define

$$\text{Loss} = (\text{LD})^2 + W|\delta E - \epsilon_0|^2, \tag{IV.2}$$

where W is a weight factor and ϵ_0 is where we want to fix δE. We then perform three rounds of optimization, increasing W from 1 to 10^9 over the rounds. This way, we first find the approximate sweet spot location, then, by increasing W, we force the optimization to fix δE to ϵ_0. The resulting value of LD can then be compared for different configurations. This will be done in Sections V.4 and V.5.

V

Results

In this section, the main results of the thesis work are presented. The results consist of analyses of both the Kitaev chain and the model of the interacting quantum dot chain presented in Chapter III. Table V.1 is provided to explain the notation of each parameter and to which model it applies.

Table V.1: Notations for each parameter in the Kitaev chain and the interacting quantum dot chain.

Kitaev chain	
ϵ	Chemical potential
$te^{i\Theta}$	Tunneling amplitude
$\Delta e^{i\Phi}$	Non-local superconducting pairing
U	Intersite Coulomb interaction
The interacting quantum dot chain	
μ	Chemical potential
w	Tunneling amplitude
Δ_{ind}	Magnitude of the induced (local) superconducting pairing
U_{intra}	Intradot Coulomb interaction
U_{inter}	Interdot Coulomb interaction
V_z	Zeeman energy
$\delta\theta$	Rotation of the magnetic field between adjacent sites
$\delta\phi$	Difference between the induced superconducting phases at adjacent sites

Except for in Section V.6, we have used homogenous superconducting phases at each site, i.e., $\delta\phi = 0$. The length of the quantum dot chain is kept to two sites, except for in Section V.5. Furthermore, $\delta\theta = \pi/2$ unless otherwise stated.

V.1 Testing the quality measures in the Kitaev chain

To test the quality measures from Section II.4.4, we apply it to the two-site Kitaev chain

$$H_{K,2} = \epsilon(n_1 + n_2) + [tc_1^\dagger c_2 + \Delta c_1^\dagger c_2^\dagger + \text{H.c.}]. \tag{V.1}$$

For simplicity, we have taken site-independent chemical potentials and positive and real t and Δ. From Eq. (II.30), we know that the sweet spot is found when $\epsilon = 0$ and $t = \Delta$. However, to get an understanding of how the LD and δE behave away from the sweet spot and to have an analytical example of the quality measures, we now determine the two curves defined by LD $= 0$ and $\delta E = 0$.

Since the Hamiltonian in Eq. (V.1) conserves number parity, i.e., if there are an odd or even number of particles in the system, we can block-diagonalize it into the two parity sectors. The odd and even parity sectors contain the states $\{|10\rangle = c_1^\dagger |00\rangle, |01\rangle = c_2^\dagger |00\rangle\}$ and $\{|00\rangle, |11\rangle = c_1^\dagger c_2^\dagger |00\rangle\}$, respectively. Diagonalizing each block leads to the ground state energies in each parity sector

$$E_o = \epsilon - t, \tag{V.2a}$$

$$E_e = \epsilon - \sqrt{\Delta^2 + \epsilon^2}. \tag{V.2b}$$

One of our sweet spot requirements is that $\delta E = 0$, i.e., that the two ground states are degenerate, which leads to the condition

$$\delta E = 0 \implies \frac{\Delta^2}{t^2} + \frac{\epsilon^2}{t^2} = 1, \tag{V.3}$$

forming a circle with radius one in the $(\Delta/t, \epsilon/t)$-plane. The sweet spot should then be located at this circle. To calculate the LD, we first determine the eigenstates corresponding to each ground state

$$|o\rangle = \frac{1}{\sqrt{2}}(|10\rangle - |01\rangle), \tag{V.4a}$$

$$|e\rangle = \frac{1}{N}\left(\frac{\Delta}{E_e}|00\rangle + |11\rangle\right), \tag{V.4b}$$

where $N^2 = 1 + \Delta^2/E_e^2$ is a normalization factor. Note that the odd state $|o\rangle$ is independent of the parameters since we take the chemical potentials of both sites to be equal. Therefore, if there is one electron in the system, the weight on each site must be equal. The density matrices for the states in Eq. (V.4) are

$$\rho^o = \frac{1}{2}(|10\rangle\langle 10| - |10\rangle\langle 01| - |01\rangle\langle 10| + |01\rangle\langle 01|) \tag{V.5a}$$

$$\rho^e = \frac{1}{N^2}\left(\frac{\Delta^2}{E_e^2}|00\rangle\langle 00| + \frac{\Delta}{E_e}|00\rangle\langle 11| + \frac{\Delta}{E_e}|11\rangle\langle 00| + |11\rangle\langle 11|\right) \tag{V.5b}$$

Taking the reduced density matrix for the first site, we get

$$\rho_1^o = \frac{1}{2}(|0\rangle\langle 0| + |1\rangle\langle 1|), \tag{V.6a}$$

$$\rho_1^e = \frac{1}{N^2}\left(\frac{\Delta^2}{E_e^2}|0\rangle\langle 0| + |1\rangle\langle 1|\right). \tag{V.6b}$$

The reduced density matrices for the second site give the same result. To get LD = 0, the odd and even reduced density matrices at each site have to be equal, and we get the condition

$$\text{LD} = 0 \implies \frac{\Delta^2}{N^2 E_e^2} = \frac{1}{N^2} = \frac{1}{2} \implies \epsilon = 0. \tag{V.7}$$

Combining this with the energy degeneracy condition in Eq. (V.3), we obtain $t = \Delta$ and see that the energy degeneracy and local indistinguishability give the expected sweet spot. See also Fig. V.1 for a numerical calculation of the two-site Kitaev chain. There, we see that LD = 0 at $\epsilon/t = 0$ and that the circle defining $\delta E = 0$ is given by Eq. (V.3). Furthermore, the numerically optimized sweet spot is located at $\epsilon = 0$ and $\Delta = t$, in accordance with theory.

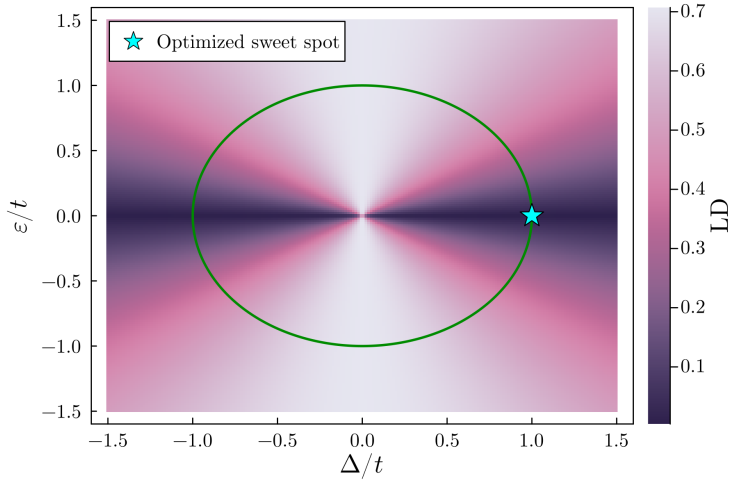

Figure V.1: Parameter scan of the two-site Kitaev chain in the $(\Delta/t, \epsilon/t)$-plane. The color scale represents the LD, and the green curve is defined by $\delta E = 0$. The star shows the numerically optimized sweet spot based on the loss function in Section II.4.4.

V.2 Checking the Kitaev limit without interactions

From Section III.2, we expect the quantum dot chain to behave like the Kitaev chain for large Zeeman energies. To confirm this, we scan the effective Kitaev-parameter Δ in Eq. (III.23) by varying $\delta\theta$ and w such that the Kitaev-tunneling amplitude t is held constant. We then perform the corresponding parameter scan in the real Kitaev chain and compare the quality measures for each model, see Fig. V.2. The

difference between the models' quality measures decreases with increasing Zeeman energies, indicating that the model has been implemented correctly.

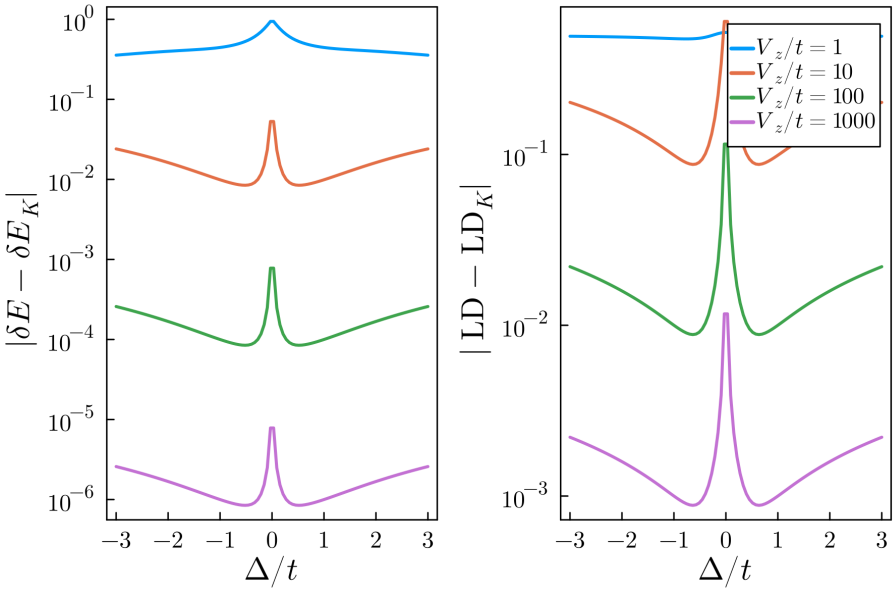

Figure V.2: Comparison of the quality measures between the two-site Kitaev chain (with subindex K) and the two-site quantum dot chain (without subindex) for varying Zeeman energies. On the x-axis are the Δ for the Kitaev model and the effective Kitaev-Δ for the quantum dot chain. The latter is scanned by varying w and $\delta\theta$, such that the effective Kitaev-t is held constant. The tunneling amplitude w varies between $\sim t - 5t$. Furthermore, $\mu = \Delta_{\mathrm{ind}} = V_z/\sqrt{2}$ such that the sweet spot condition $\epsilon = 0$ is fulfilled.

To reach the sweet spot, the effective Kitaev-parameters in Eq. (III.23) must fulfill the conditions $\epsilon = 0$ and $t = \Delta$. The first condition (which we have seen is equivalent with $\mathrm{LD} = 0$) means that

$$\epsilon = 0 \implies \beta = \sqrt{\mu^2 + \Delta_{\mathrm{ind}}^2} = V_z. \tag{V.8}$$

The sweet spot, therefore, lies on a circle with radius V_z/w in the $(\Delta_{\mathrm{ind}}/w, \mu/w)$-plane. The induced superconductivity must hence scale with the Zeeman splitting to reach the sweet spot. We discuss this further in Section V.4. The second condition gives

$$t = \Delta \implies \frac{\mu}{\Delta_{\mathrm{ind}}} = \left|\tan\frac{\delta\theta}{2}\right|, \tag{V.9}$$

and the sweet spot, therefore, lies at an angle $\delta\theta/2$ from the Δ_{ind} axis. To confirm this numerically, we perform the optimization procedure for a large Zeeman energy and check if the sweet spot is located at this expected position. In Fig. V.3, this is done for two sites with a Zeeman energy of $V_z = 50w$. The optimized sweet spot is seen to coincide with the above theory, valid for $V_z \gg w$.

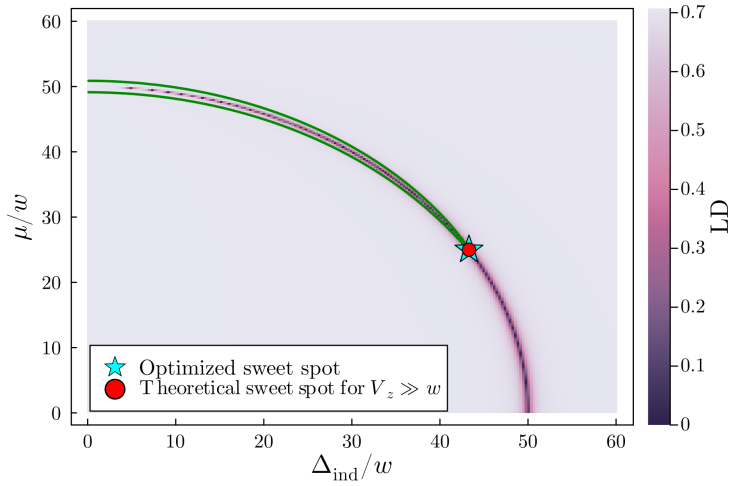

Figure V.3: Parameter scan of the two-site quantum dot chain in the $(\Delta_{\mathrm{ind}}/w, \mu/w)$-plane using $\delta\theta = \pi/3$ and $V_z = 50w$. The color scale represents the LD, and the green curve is defined by $\delta E = 0$. The blue star shows the numerically optimized sweet spot and the red dot indicates the location of the sweet spot in the Kitaev limit $V_z \gg w$.

To understand the plot in Fig. V.3 better, we can translate the conditions for $\delta E = 0$ and $\mathrm{LD} = 0$ for the two-site Kitaev chain given by Eqs. (V.3) and (V.7) into the system parameters. Since the conditions $\mathrm{LD} = 0$ and $\epsilon = 0$ are equivalent, the LD-condition is given in Eq. (V.8), and forms the previously mentioned circle with radius V_z/w in the $(\Delta_{\mathrm{ind}}/w, \mu/w)$-plane. A quarter of this circle can be seen in Fig. V.3. The condition for $\delta E = 0$ becomes

$$\left(\sqrt{\mu^2 + \Delta_{\mathrm{ind}}^2} - V_z\right)^2 + \frac{w^2\Delta_{\mathrm{ind}}^2}{V_z^2}\sin^2\frac{\delta\theta}{2} = \frac{w^2\mu^2}{V_z^2}\cos^2\frac{\delta\theta}{2}. \tag{V.10}$$

In Fig. V.4, the analytical curves in Eqs. (V.8) and (V.10) are plotted for the same parameters as in Fig. V.3.

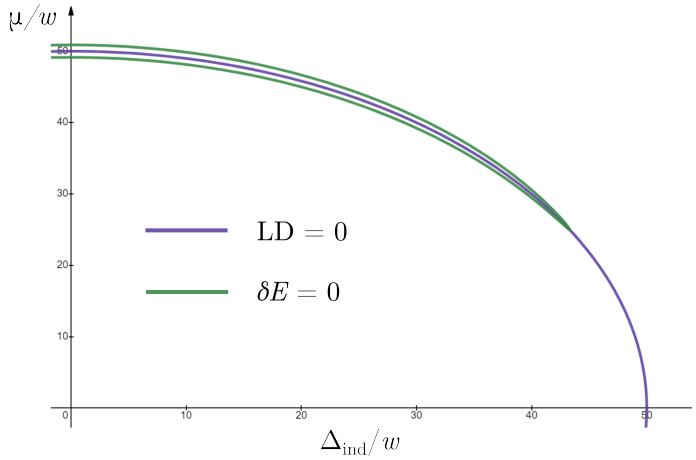

Figure V.4: The curves $\mathrm{LD} = 0$ and $\delta E = 0$ defined by Eqs. (V.8) and (V.10) for the same parameters as in Fig. V.3.

V.3 Including interactions

In this section, we will start to include Coulomb interactions. In the initial Hamiltonian of the model in Eqs. (III.1) and (III.2), we have included interactions between electrons on the same dot (intradot) and neighboring dots (interdot). Firstly, we will see how the intradot Coulomb interaction looks after projecting it on the states without b-excitations. Next, we will study intersite interactions in the two-site Kitaev chain and show that a sweet spot ($\delta E = \mathrm{LD} = 0$) still exists.

V.3.1 Intradot interactions

To see how intradot Coulomb interactions affect the Kitaev limit, we follow the same procedure as in Section III.2. It is important to note that the interaction is between the original electrons defined by the d-operators and not between the a- and b-particles. Therefore, we must take the transformation between the $\tilde{d}$-operators and the a- and b-operators in Eq. (III.19) and insert this into the intradot Coulomb interaction term in Eq. (III.9). For large magnetic fields, we can then project the resulting Hamiltonian on the states without b-excitations. The result is an extra term

$$H_{\text{intra}} = -\frac{U_{\text{intra}}}{2}\left(1 - \frac{\mu}{\beta}\right)\sum_j a_j^\dagger a_j, \tag{V.11}$$

which renormalizes the Kitaev chemical potential in Eq. (III.23a) to

$$\epsilon = \sqrt{\mu^2 + \Delta_{\text{ind}}^2} - V_z - \frac{U_{\text{intra}}}{2}\left(1 - \frac{\mu}{\sqrt{\mu^2 + \Delta_{\text{ind}}^2}}\right). \tag{V.12}$$

V.3.2 Interdot interactions

Before adding interdot Coulomb interactions to our system, we want to understand it in a simpler case – an interacting two-site Kitaev chain. Starting with Eq. (V.1), we add an intersite Coulomb interaction U to the Hamiltonian such that

$$H_{K,2} + H_U = \epsilon(n_1 + n_2) + [tc_1^\dagger c_2 + \Delta c_1^\dagger c_2^\dagger + \text{H.c.}] + Un_1n_2. \tag{V.13}$$

Now, the Hamiltonian is not a Kitaev chain anymore, and we cannot use the conditions $t = \Delta$ and $\epsilon = 0$ in Eq. (II.30) to determine where the sweet spot is. So instead, we will use our quality measures.

Following the same procedure as in Section V.1, we block-diagonalize the system and find the ground states in the odd and even parity sectors. However, we can restrict ourselves to the even sector since the Coulomb interaction does not affect the odd parity states. The odd parity states with intersite Coulomb interactions are

hence the same as in Section V.1. The energy of the even ground state becomes

$$E_e = \epsilon + \frac{U}{2} - \sqrt{\left(\epsilon + \frac{U}{2}\right)^2 + \Delta^2}, \tag{V.14}$$

and the corresponding eigenstate is the same as in Eq. (V.4b), but with E_e from Eq. (V.14). The sweet spot conditions of degenerate ground states and equal reduced density matrices become

$$\delta E = 0 \implies \frac{\Delta^2}{t^2} + \left(\frac{\epsilon}{t} + \frac{U}{2t}\right)^2 = \left(\frac{U}{2t} + 1\right)^2, \tag{V.15a}$$

$$\mathrm{LD} = 0 \implies \epsilon = -\frac{U}{2}. \tag{V.15b}$$

The first condition forms a circle in the $(\Delta/t, \epsilon/t)$-plane, centered at $(0, -U/2t)$ and a radius of $U/2t + 1$. The second condition forms a horizontal line at $\epsilon/t = -U/2t$ in the same plane. At the point $(U/2t + 1, -U/2t)$, both conditions are fulfilled. Therefore, despite intersite Coulomb interactions in the Kitaev chain, a sweet spot based on our quality measures can still be found. This conclusion corrects the result in Ref. [17], where it was stated that intersite Coulomb interactions destroyed the possibility of sweet spots. See Fig. V.5 for a numerical calculation of the Kitaev chain with interdot interactions. Again, the numerically optimized sweet spot coincides with the theory.

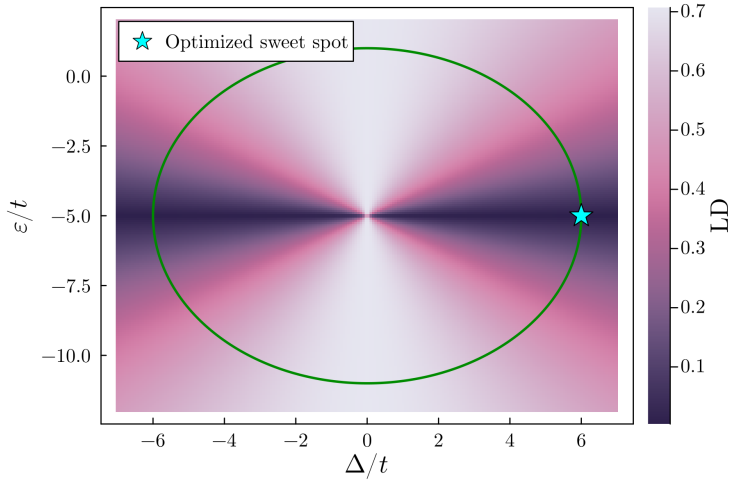

Figure V.5: The same plot as Fig. V.1 but with a finite intersite Coulomb interaction ($U = 10t$). The numerically optimized sweet spot coincides with the algebraic result $(U/2t + 1, -U/2t) = (6, -5)$.

Adding interdot Coulomb interactions to the quantum dot chain and translating it into a- and b-operators, terms of the form $a_{j+1}^\dagger a_{j+1} a_j^\dagger a_j$ appear after the projection on the states without b-excitations. The system hence reduces to a Kitaev chain with intersite Coulomb interactions. Based on the above calculation, we expect

that a good-quality sweet spot can still be found in the quantum dot chain for large magnetic fields. However, we expect the sweet spot to move compared to the theory in Section V.2.

After projecting the Hamiltonian onto the states with no b-excitations, there also appear terms that renormalize the chemical potentials of the quantum dots, similarly to Section V.3.1. These terms affect the sites on the ends differently than the ones in the middle of the chain. Therefore, the chemical potentials have to be tuned differently along the chain to reach the sweet spot. However, studying this case was outside the scope of the present work.

V.4 Reducing the magnetic field

As discussed in Section II.4.3, there is a limit to how large the Zeeman energy can get in an experiment since large magnetic fields destroy superconductivity. Additionally, in our system, there is another restriction to the magnetic field. Since one of the requirements for a sweet spot in Eq. (V.10) is that $\mu^2 + \Delta_{\text{ind}}^2 = V_z^2$, the induced superconducting pairing must increase with the Zeeman energy at the sweet spot. However, as discussed in Section II.3.2, Δ_{ind} is bounded by the superconducting gap in the parent superconductor. Therefore, for large enough Zeeman energies, Δ_{ind} cannot be large enough to reach the sweet spot.

Due to the restrictions of the magnetic field strength, it is of interest to track the quality of MBSs at the optimized sweet spot while lowering the magnetic field. This allows us to see how this quality scales with the Zeeman energy and determine how large it must be to reach a certain MBS quality. In Fig. V.6, the optimization procedure in Section IV.1 has been performed for a chain of two sites with different combinations of included interactions and varying magnetic fields.

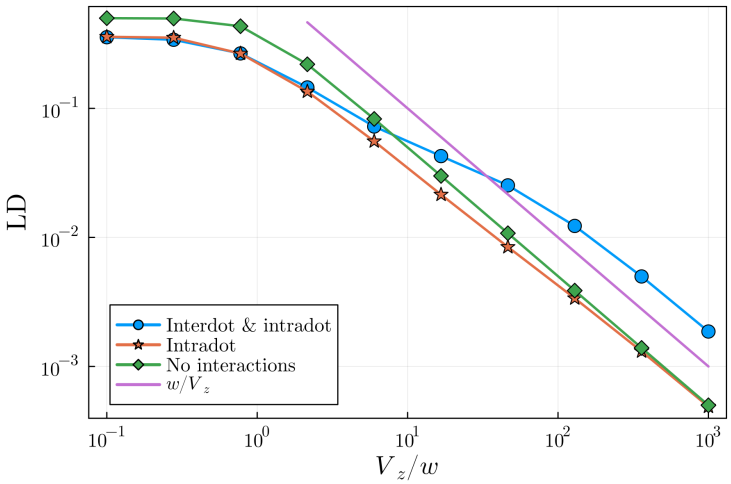

Figure V.6: The LD on a logarithmic scale for varying Zeeman energies at the optimized sweet spot using the optimization procedure in Section IV.1. Due to the optimization procedure, $\delta E \approx 10^{-7}$ at each point. The different curves represent different combinations of included intradot and interdot Coulomb interactions. The values used for the interactions are $U_{\text{intra}} = 100w$ and $U_{\text{inter}} = 20w$. An additional curve defined by w/V_z is given for reference.

A few conclusions can be made based on Fig. V.6. Firstly, for large Zeeman energies, the LD improves as w/V_z for all curves. Secondly, intradot Coulomb interactions improve the LD. This might be because the intradot interactions help the Zeeman splitting to push the b-excitations further away in energy. However, for large Zeeman energies, the difference due to intradot interactions is less noticeable. Finally, interdot Coulomb interactions worsen the LD for large Zeeman energies. However, the LD still approaches zero as V_z increases. This can be explained by the analysis in Section V.3.2, where we showed that sweet spots in an interacting Kitaev chain could be found.

Instead of increasing V_z to obtain higher quality MBSs, one could lower the tunneling amplitude w. However, as mentioned in Section II.4.3, the gap to the next excited states is given by $E_{\text{gap}} = 2t$, where t is the Kitaev tunneling amplitude. According to Eq. (III.23), t is proportional to w, and hence, by decreasing w, the gap to the next excited states also reduces. To detect MBSs, the gap cannot be too small, e.g., compared to the temperature. Therefore, the tunneling amplitude cannot be decreased indefinitely.

V.5 Adding more dots to the chain

In this section, we add more sites to the model, increasing it to three and four sites. In Fig. V.7, the same calculation as in Fig. V.6 has been made, but with varying numbers of sites in the chain.

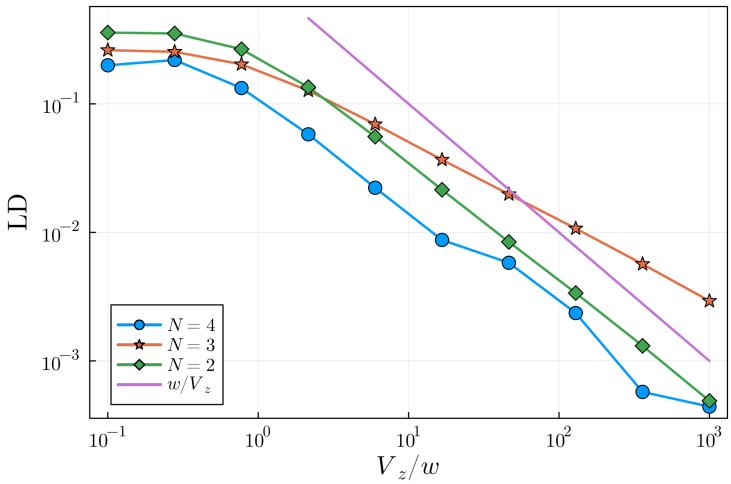

Figure V.7: The same plot as in Fig. V.6 but with varying numbers of sites in the quantum dot chain. For each curve, $U_{\text{intra}} = 100w$ and $U_{\text{inter}} = 0$. Again, the energy degeneracy is kept at $\approx 10^{-7}$.

According to Fig. V.7, adding more sites to the chain does not necessarily decrease the LD. The chain with $N = 3$ has a larger LD than $N = 2$. Furthermore, the scaling with Zeeman energy is worse for $N = 3$. However, when increasing the chain length to four sites, the LD is better than the shorter chains, although with similar scaling as the two-site chain. The $N = 4$ curve is less smooth than the other curves. This, we believe, is because of the increased computational cost of the larger system, which leads to fewer function evaluations in the optimization procedure than the smaller systems. To counteract this, the optimization procedures for the larger systems were run for longer times, but for $N = 4$, it might not have been enough for complete convergence.

When including interdot Coulomb interactions, there were convergence issues for the chains with $N > 2$. One reason might be that the interdot interaction term renormalizes the chemical potentials differently at the sites at the ends of the chain compared to the ones in the middle with two neighboring sites, as discussed in Section V.3.2. Therefore, the best sweet spot could lie outside of our optimization region since we only consider homogenous chemical potentials. However, including inhomogeneous chemical potentials was outside this thesis's scope.

V.6 Tuning using superconducting phase

As mentioned in Section II.4.3, to create poor man's MBSs in short Kitaev-chains, it is crucial that the system can be fine-tuned to the sweet spot. One experimentally reachable degree of freedom in the quantum dot chain is the chemical potentials of the quantum dots since gate electrodes easily tune them. This could be used to satisfy $\epsilon = 0$. However, we need also to be able to tune the ratio t/Δ, see

Eq. (III.23). This could be done by controlling the rotation of the magnetic fields $\delta\theta$, as was proposed in the original poor man's model [17]. However, this is tricky to realize experimentally. Furthermore, if the rotation of the magnetic fields is replaced by spin-orbit coupling, it would be impossible to tune. It would therefore be preferable if a different mechanism could tune the t/Δ-ratio.

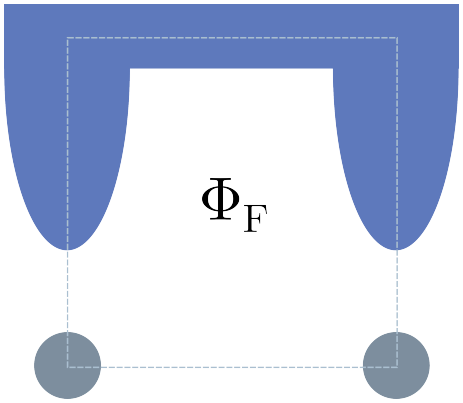

Figure V.8: By applying a magnetic flux Φ_F through the dashed loop, the phase difference between the induced superconductivity $\delta\phi$ can be controlled [2].

During the work of the thesis, it was realized that the ability to control the phase difference between the superconductors could act as a different tuning knob for the t/Δ-ratio. This could be done by applying a magnetic flux through a loop connecting the superconductors, see Fig. V.8. When including differences in the superconducting phases between the sites, i.e., $\delta\phi \neq 0$, the effective Kitaev parameters t and Δ become

$$t = \frac{w\sqrt{\mu^2 + V_z^2 - \Delta_{\text{ind}}^2 \cos\delta\phi}}{\sqrt{2}V_z} \left|\cos\frac{\delta\theta}{2}\right|, \tag{V.16a}$$

$$\Delta = \frac{w\Delta_{\text{ind}}}{V_z} \left|\sin\frac{\delta\theta}{2}\right| \left|\cos\frac{\delta\phi}{2}\right|, \tag{V.16b}$$

where we have inserted $\beta = V_z$ to satisfy $\epsilon = 0$. Furthermore, no interactions have been taken into account. From Eq. (V.16), we can see that t increases when varying $\delta\phi$ from zero, while Δ decreases. If we initially have the same superconducting phases at each site ($\delta\phi = 0$) and a large rotation between the magnetic fields ($\delta\theta \approx \pi$), the system is initialized such that $t < \Delta$. A superconducting phase difference could then be applied to satisfy $t = \Delta$ and reach the sweet spot.

VI

Conclusion

In this thesis, we have analyzed an interacting chain of quantum dots proximitized by superconductors for its potential to host MBSs. In Chapter III, we did the derivation sketched in Ref. [1] to show that, for large Zeeman energies, the non-interacting system reduces to a Kitaev chain with effective Kitaev-parameters in Eq. (III.23). The main novel contribution of this thesis was to add interactions to the system. To test the quality of the MBSs when including interactions and when away from the ideal set of parameters, we developed quality measures for the MBSs in Section II.4.4. Since perfect MBSs result in degenerate and locally indistinguishable ground states, these two properties were used as quality measures.

The measures were then used to numerically optimize for the best sweet spot for a given set of parameters and evaluate its quality. Performing the optimization procedure for the two-site quantum dot chain with varying Zeeman energies and different combinations of included interactions, we could conclude that intradot interactions improve the quality of the MBSs. In contrast, interdot interactions worsen it, see Fig. V.6. However, even when including interdot interactions, the LD approaches zero when increasing the Zeeman energy, and high-quality MBSs can still be found. We also studied the MBS quality when adding more dots to the chain, which would intuitively allow the MBSs to be more separated. However, as shown in Fig. V.7, the LD for the three-site chain is higher and has a worse scaling with the Zeeman energy than the two-site chain. Finally, we discussed how to tune the system to a sweet spot experimentally. In particular, we showed that the t/Δ-ratio can be tuned by applying an additional magnetic field to control the superconducting phase difference between the superconductors.

Since the quantum dot chain consists of quantum dots directly neighboring each other, it would be problematic if interdot Coulomb interactions would destroy the possibility of finding high-quality MBSs. However, the novel finding that interdot interactions still leave the possibility of sweet spots, combined with the potential

of tuning the system using the superconducting phases, means that the quantum dot chain is highly relevant for creating and detecting MBSs experimentally. Furthermore, the two-site chain is probably the system to focus on since the reward for adding one or two more dots does not seem to be worth the extra experimental effort. An important next step when continuing this project would be to propose a detailed tuning procedure to reach the sweet spot and detect MBSs in an experiment. Also, it would be interesting to determine what MBS quality can be achieved for experimentally appropriate parameter values. We expect that good-quality MBSs are necessary to detect the exotic properties of MBSs, such as the protection against local perturbations and non-Abelian exchange statistics. However, precisely what the required values of LD and δE are is a subject of current research.

To conclude, the simplicity of using quantum dots to create and detect MBSs is appealing and has brought new life to the search for MBSs. Creating poor man's MBSs in quantum dot chains, such as the one considered in this thesis, would be a crucial step toward developing topological quantum computing and an exciting discovery for those amazed by the exotic physics MBSs promises.

Bibliography

[1] I. C. Fulga, A. Haim, A. R. Akhmerov, and Y. Oreg, "Adaptive tuning of Majorana fermions in a quantum dot chain", New Journal of Physics **15**, Publisher: IOP Publishing, 045020 (2013).

[2] M. Tinkham, *Introduction to superconductivity*, 2. ed (McGraw Hill, 1996).

[3] D. W. Snoke, *Solid State Physics: Essential Concepts* (Cambridge University Press, 2020).

[4] R. Hanson, L. P. Kouwenhoven, J. R. Petta, S. Tarucha, and L. M. K. Vandersypen, "Spins in few-electron quantum dots", Reviews of Modern Physics **79**, arXiv:cond-mat/0610433, 1217–1265 (2007).

[5] Y. Oreg, G. Refael, and F. Von Oppen, "Helical Liquids and Majorana Bound States in Quantum Wires", Physical Review Letters **105**, 177002 (2010).

[6] J. Alicea, "New directions in the pursuit of Majorana fermions in solid state systems", Reports on Progress in Physics **75**, Publisher: IOP Publishing, 076501 (2012).

[7] M. Leijnse and K. Flensberg, "Introduction to topological superconductivity and Majorana fermions", Semiconductor Science and Technology **27**, Publisher: IOP Publishing, 124003 (2012).

[8] E. Gibney, "Inside Microsoft's quest for a topological quantum computer", Nature, Publisher: Nature Publishing Group, 10.1038/nature.2016.20774 (2016).

[9] V. Mourik, K. Zuo, S. M. Frolov, S. R. Plissard, E. P. A. M. Bakkers, and L. P. Kouwenhoven, "Signatures of Majorana Fermions in Hybrid Superconductor-Semiconductor Nanowire Devices", Science **336**, Publisher: American Association for the Advancement of Science, 1003–1007 (2012).

[10] M. T. Deng, C. L. Yu, G. Y. Huang, M. Larsson, P. Caroff, and H. Q. Xu, "Anomalous Zero-Bias Conductance Peak in a Nb–InSb Nanowire–Nb Hybrid Device", Nano Letters **12**, Publisher: American Chemical Society, 6414–6419 (2012).

[11]M. T. Deng, S. Vaitiekėnas, E. B. Hansen, J. Danon, M. Leijnse, K. Flensberg, J. Nygård, P. Krogstrup, and C. M. Marcus, "Majorana bound state in a coupled quantum-dot hybrid-nanowire system", Science **354**, Publisher: American Association for the Advancement of Science, 1557–1562 (2016).

[12]S. Vaitiekėnas, G. W. Winkler, B. van Heck, T. Karzig, M.-T. Deng, K. Flensberg, L. I. Glazman, C. Nayak, P. Krogstrup, R. M. Lutchyn, and C. M. Marcus, "Flux-induced topological superconductivity in full-shell nanowires", Science **367**, Publisher: American Association for the Advancement of Science, eaav3392 (2020).

[13]G. Kells, D. Meidan, and P. W. Brouwer, "Near-zero-energy end states in topologically trivial spin-orbit coupled superconducting nanowires with a smooth confinement", Physical Review B **86**, 100503 (2012).

[14]O. A. Awoga, J. Cayao, and A. M. Black-Schaffer, "Supercurrent Detection of Topologically Trivial Zero-Energy States in Nanowire Junctions", Physical Review Letters **123**, 117001 (2019).

[15]H. Pan and S. Das Sarma, "Physical mechanisms for zero-bias conductance peaks in Majorana nanowires", Physical Review Research **2**, Publisher: American Physical Society, 013377 (2020).

[16]A. Y. Kitaev, "Unpaired Majorana fermions in quantum wires", Physics-Uspekhi **44**, 131 (2001).

[17]M. Leijnse and K. Flensberg, "Parity qubits and poor man's Majorana bound states in double quantum dots", Physical Review B **86**, 134528 (2012).

[18]A. Tsintzis, R. S. Souto, and M. Leijnse, "Creating and detecting poor man's Majorana bound states in interacting quantum dots", Physical Review B **106**, Publisher: American Physical Society, L201404 (2022).

[19]T. Dvir, G. Wang, N. van Loo, C.-X. Liu, G. P. Mazur, A. Bordin, S. L. D. ten Haaf, J.-Y. Wang, D. van Driel, F. Zatelli, X. Li, F. K. Malinowski, S. Gazibegovic, G. Badawy, E. P. A. M. Bakkers, M. Wimmer, and L. P. Kouwenhoven, "Realization of a minimal Kitaev chain in coupled quantum dots", Nature **614**, Number: 7948 Publisher: Nature Publishing Group, 445–450 (2023).

[20]L. P. Kouwenhoven, D. G. Austing, and S. Tarucha, "Few-electron quantum dots", Reports on Progress in Physics **64**, 701 (2001).

[21]C. Fasth, A. Fuhrer, M. T. Björk, and L. Samuelson, "Tunable Double Quantum Dots in InAs Nanowires Defined by Local Gate Electrodes", Nano Letters **5**, 1487–1490 (2005).

[22]J. Bardeen, L. N. Cooper, and J. R. Schrieffer, "Microscopic Theory of Superconductivity", Physical Review **106**, 162–164 (1957).

[23]N. N. Bogoljubov, "On a new method in the theory of superconductivity", Il Nuovo Cimento (1955-1965) **7**, 794–805 (1958).

[24]J. G. Valatin, "Comments on the theory of superconductivity", Il Nuovo Cimento (1955-1965) **7**, 843–857 (1958).

[25]P.-G. d. Gennes, *Superconductivity of metals and alloys*, Frontiers in physics (1966).

[26]L. N. Cooper, "Bound Electron Pairs in a Degenerate Fermi Gas", Physical Review **104**, Publisher: American Physical Society, 1189–1190 (1956).

[27]E. Maxwell, "Isotope Effect in the Superconductivity of Mercury", Physical Review **78**, Publisher: American Physical Society, 477–477 (1950).

[28]C. A. Reynolds, B. Serin, W. H. Wright, and L. B. Nesbitt, "Superconductivity of Isotopes of Mercury", Physical Review **78**, Publisher: American Physical Society, 487–487 (1950).

[29]M. Sato and Y. Ando, "Topological superconductors: a review", Reports on Progress in Physics **80**, Publisher: IOP Publishing, 076501 (2017).

[30]A. F. Andreev, "The thermal conductivity of the intermediate state in superconductors", Zhurnal Eksperimental'noj I Teoreticheskoj Fiziki **46** (1964).

[31]T. Yoshioka and Y. Ohashi, "Numerical Renormalization Group Studies on Single Impurity Anderson Model in Superconductivity: A Unified Treatment of Magnetic, Nonmagnetic Impurities, and Resonance Scattering", Journal of the Physical Society of Japan **69**, Publisher: The Physical Society of Japan, 1812–1823 (2000).

[32]J. Bauer, A. Oguri, and A. C. Hewson, "Spectral properties of locally correlated electrons in a Bardeen–Cooper–Schrieffer superconductor", Journal of Physics: Condensed Matter **19**, 486211 (2007).

[33]T. Meng, S. Florens, and P. Simon, "Self-consistent description of Andreev bound states in Josephson quantum dot devices", Physical Review B **79**, Publisher: American Physical Society, 224521 (2009).

[34]M. Kjaergaard, K. Wölms, and K. Flensberg, "Majorana fermions in superconducting nanowires without spin-orbit coupling", Physical Review B **85**, 020503 (2012).

[35]J. D. Sau and S. D. Sarma, "Realizing a robust practical Majorana chain in a quantum-dot-superconductor linear array", Nature Communications **3**, Number: 1 Publisher: Nature Publishing Group, 964 (2012).

[36]G. Schaller, *Open Quantum Systems Far from Equilibrium*, Vol. 881, Lecture Notes in Physics (Springer International Publishing, 2014).

[37]T.-P. Choy, J. M. Edge, A. R. Akhmerov, and C. W. J. Beenakker, "Majorana fermions emerging from magnetic nanoparticles on a superconductor without spin-orbit coupling", Physical Review B **84**, 195442 (2011).

[38]Julia, *The Julia Programming Language*, https://julialang.org/ (visited on 05/29/2023).

[39]V. Svensson and W. Samuelson, *QuantumDots.jl*, https://github.com/cvsvensson/QuantumDots.jl/, (Developed by Viktor Svensson, with a little assistance from the author), GitHub repository, 2023.

[40]R. Feldt, *Blackboxoptim.jl*, https://juliapackages.com/p/blackboxoptim (visited on 05/29/2023).

[41]W. Samuelson, *MajoranaQDchain*, https://github.com/williamesamuelson/majoranaQDchain, GitHub repository, 2023.

A

Appendix

A.1 Andreev bound states

In this section, we analyze the Hamiltonian in Eq. (II.20) describing a quantum dot proximitized by a superconductor and the formation of Andreev bound states. Due to the last term in Eq. (II.20), the effective Hamiltonian does not conserve the number of particles on the dot. However, it conserves the system's parity, i.e., if there is an even or odd number of electrons on the dot. We can hence block-diagonalize the Hamiltonian in terms of the odd and even parity sector to obtain the eigenstates and eigenenergies. For the odd parity sector, the eigenstates are simply $|\uparrow\rangle$ and $|\downarrow\rangle$ with degenerate energies $E_{\uparrow,\downarrow} = \epsilon_{\mathrm{QD}}$. Due to the degeneracy, these states are usually called doublets. In the even parity section, the eigenstates and eigenenergies are

$$\begin{aligned} |+\rangle &= u\,|0\rangle + v\,|\uparrow\downarrow\rangle\,, \quad E_+ = \xi_{\mathrm{QD}} + \sqrt{\xi_{\mathrm{QD}}^2 + \Gamma^2} \\ |-\rangle &= v\,|0\rangle - u\,|\uparrow\downarrow\rangle\,, \quad E_- = \xi_{\mathrm{QD}} - \sqrt{\xi_{\mathrm{QD}}^2 + \Gamma^2}, \end{aligned} \tag{A.1}$$

where $\xi_{\mathrm{QD}} = \epsilon_{\mathrm{QD}} + U/2$ and u, v are scalars. These states are called BCS singlets since they, similarly to the BCS ground state in Eq. (II.2), are superpositions of states with an even number of electrons.

Depending on the parameters $\epsilon_{\mathrm{QD}}, U$ and Γ, the ground state of the proximitized quantum dot is either odd (one of the doublets) or even (the BCS singlet $|-\rangle$). The energy required to excite the system from the ground state is given by $\delta E = |E_- - E_{\uparrow,\downarrow}| = |U/2 - \sqrt{\xi_{\mathrm{QD}}^2 + \Gamma^2}|$. Since Δ is assumed to be the largest energy scale in the system, this excited state lies within the superconducting gap, where there in a bulk superconductor are no states. Such a subgap state is called an Andreev bound state [32, 33].